Modeling aerosol formation in alpha-pinene photo-oxidation experiments

M. Capouet,[1,2] J.-F. Müller,[1] K. Ceulemans,[1] S. Compernolle,[1] L. Vereecken,[3] and J. Peeters[3]

Received 21 May 2007; revised 29 August 2007; accepted 23 October 2007; published 29 January 2008.

[1] We present BOREAM (Biogenic hydrocarbon Oxidation and Related Aerosol formation Model), a detailed model for the oxidation of α-pinene and the resulting formation of secondary organic aerosol (SOA). It is based on a quasi-explicit gas phase mechanism for the formation of primary products, developed on objective grounds using advanced theoretical methods, and on a simplified representation for the further oxidation of the products. The partitioning of the products follows a kinetic representation with coefficients estimated from vapor pressures calculated using a dedicated group contribution method. Particle phase and heterogeneous reactions are generally neglected, but the impact of peroxyhemiacetal formation in the aerosol is tested on the basis of laboratory estimates of the reaction rates. The model is evaluated against 28 laboratory experiments from 6 studies of α-pinene photo-oxidation covering a wide range of photochemical conditions. In contrast with previous modeling studies, the modeled and measured SOA yields agree to within a factor of 2 in most cases. The SOA yields are underestimated for the ozonolysis experiments of Presto et al. (2005a) when the standard version of the ozonolysis mechanism is used, presumably because of the lack of credible pathways for the formation of pinic and hydroxy pinonic acid. The underestimation is drastically reduced when the mechanism is modified to account for the formation of these compounds. Accounting for peroxyhemiacetal formation in the particle phase is found to further increase the SOA yields by about one third in high VOC ozonolysis experiments and to have a much smaller impact in all other cases. The model calculates that ozonolysis contributes about twice more to SOA formation than oxidation by OH, whereas NO_3-initiated oxidation is negligible. In agreement with previous studies, low NO_x conditions and low temperatures are calculated to favor aerosol formation, but the estimated temperature dependence is stronger than found in recent laboratory experiments.

Citation: Capouet, M., J.-F. Müller, K. Ceulemans, S. Compernolle, L. Vereecken, and J. Peeters (2008), Modeling aerosol formation in alpha-pinene photo-oxidation experiments, *J. Geophys. Res.*, *113*, D02308, doi:10.1029/2007JD008995.

1. Introduction

[2] The atmospheric oxidation of biogenic monoterpenes is believed to be an important source of low-volatility products which can partition between the gas and particle phases, and therefore contribute to the organic aerosol burden [e.g., *Seinfeld and Pandis*, 1998]. The least volatile among the oxidation products are even susceptible to nucleate and generate new particles [*Koch et al.*, 2000; *Bonn and Moortgat*, 2002]. Among the monoterpenes, α-pinene is the most largely emitted compound [*Guenther et al.*, 1995], and also the compound which has received the most attention. Since the pioneering work of *Hatakeyama et al.* [1991], a large number of laboratory studies have attempted to quantify the formation of secondary organic aerosol (SOA) and to characterize its dependence on photochemical conditions (e.g., initial concentration of precursors and nitrogen oxides), temperature, and other factors [e.g., *Hoffmann et al.*, 1997; *Griffin et al.*, 1999a; *Kamens and Jaoui*, 2001; *Takekawa et al.*, 2003; *Presto et al.*, 2005a, 2005b; *Ng et al.*, 2006; *Pathak et al.*, 2007]. On the basis of such observations and the absorptive partitioning theory of *Pankow* [1994a], simple representations of SOA formation have been implemented in atmospheric models in order to provide first-hand estimates of the monoterpene impact on the aerosol load of the atmosphere on a global scale [e.g., *Griffin et al.*, 1999b; *Kanakidou et al.*, 2000; *Chung and Seinfeld*, 2002; *Derwent et al.*, 2003; *Lack et al.*, 2004; *Tsigaridis et al.*, 2005] or a regional scale [*Anderson-Sköld and Simpson*, 2001; *Griffin et al.*, 2002], but they ignore the complexity of the processes underlying SOA formation and the fact that the laboratory conditions are most often too different from atmospheric conditions to allow straightfor-

[1]Belgian Institute for Space Aeronomy, Brussels, Belgium.
[2]Now at Belgian Agency for Radioactive Waste and Enriched Fissile Materials, Brussels, Belgium.
[3]Department of Chemistry, University of Leuven, Heverlee, Belgium.

0148-0227/08/2007JD008995

ward extrapolation [*Seinfeld and Pankow*, 2003]. Unfortunately, the realization of a fully explicit chemical degradation mechanism of a monoterpene appears out of reach in the near future, since it would probably require the characterization of millions (maybe billions) of reactions [*Aumont et al.*, 2005]. Furthermore, recent theoretical work [e.g., *Peeters et al.*, 2001; *Capouet et al.*, 2004; *Vereecken et al.*, 2007] (see also section 2.2) indicates that unexpected reaction sequences frequently occur, often involving the isomerization of oxy or peroxy radicals, which cannot be predicted by current protocols for mechanism development. The theoretical characterization of even a single reaction can, in some cases, require high-level methods and substantial computing capabilities. For these reasons, explicit α-pinene oxidation mechanisms can, at best, describe the first oxidation steps, and the rest of the mechanism has to be parameterized. It is a reasonable hope that the first stage of an α-pinene oxidation experiment (typically a few hours) can be described accurately on the basis of such a partial mechanism, and that the nonexplicit, further oxidation of the stable products plays only a minor role in that time period. This approach has been successfully applied in the simulation of the evolution of gas phase species in α-pinene OH-initiated oxidation experiments [*Capouet et al.*, 2004]. The simulation of aerosol formation in photo-oxidation experiments of α-pinene represents a more challenging objective, for several reasons. Firstly, although ozonolysis has been identified as the most efficient route to SOA production [*Griffin et al.*, 1999a], the formation pathways of supposedly crucial ozonolysis products like pinic acid and hydroxy pinonic acid remain so far nonelucidated (see section 2.2). Secondly, the saturation vapor pressures of the products, required to estimate their partitioning between the gas and aerosol phases, are highly uncertain, in particular in the case of low-volatility polyfunctional compounds [*Capouet and Müller*, 2006]. Finally, the SOA yields are known from laboratory investigations to depend on the presence and nature of seed particles, and on the presence of water [*Jang and Kamens*, 1998; *Fick et al.*, 2003; *Gao et al.*, 2004], suggesting that particle phase reactions favored by elevated acidity levels play an important role and contribute to particle growth.

[3] This article presents the BOREAM model (Biogenic hydrocarbon Oxidation and Related Aerosol formation Model) which describes the oxidation of α-pinene and the resulting formation of secondary organic aerosol (SOA). It is based on a comprehensive gas phase mechanism built on our previous work [*Peeters et al.*, 2001; *Capouet et al.*, 2004]. The formation of stable (primary) products is described explicitly, as well as the further oxidation of pinonaldehyde, a known major primary product (section 2.2). The oxidation mechanism of the other primary products is also included, although in a less detailed form (section 2.3). The gas/particle partitioning of the condensable products is calculated on the basis of vapor pressures estimated from a group contribution method [*Capouet and Müller*, 2006] (section 2.4). Heterogeneous and particle phase reactions are generally neglected, except for the formation of peroxyhemiacetals from the reaction of aldehydes and hydroperoxides in the aerosol [*Antonovskii and Terent'ev*, 1967], which has been suggested in a modeling study [*Johnson et al.*, 2005] to strongly enhance SOA formation from the oxidation of aromatic compounds. The acid-catalyzed formation of such compounds from gaseous aldehydes with particulate hydroperoxides has been suggested to occur by *Tobias and Ziemann* [2000] in the ozonolysis of 1-tetradecene. Although many other processes have been invoked in order to explain the observed formation of oligomers in SOA particles [*Jang and Kamens*, 1998; *Kalberer et al.*, 2004; *Gao et al.*, 2004], their role should be limited in the case of laboratory experiments conducted at low relative humidities, with no acidic seed, and with sampling times generally not exceeding about 5 hours. In any case, their speculative nature, and the large uncertainties regarding the kinetics for their elementary steps make it extremely difficult to provide reliable model representations for these processes.

[4] The complete mechanism of the BOREAM model, i.e., the gas phase mechanism and the partitioning (adsorption and desorption) reactions can be explored at http://www.oma.be/TROPO/boream/boream.html. It includes a total of $\sim$5000 reactions and 1300 species. The continuity equations for the chemical species are solved by a Rosenbrock scheme of order 4 embedded in the "KPP" (Kinetic Pre-Processor) package [*Damian-Iordache et al.*, 1995].

[5] The model is tested against measured SOA yields in laboratory experiments in section 3. Ozonolysis experiments conducted in the dark and in absence of NO*x* [e.g., *Yu et al.*, 1999] are not considered, in part because of the still preliminary nature of our ozonolysis mechanism, and also because the nighttime ozonolysis of α-pinene can be considered as relatively marginal in the real atmosphere, as shown in section 2.1. The effects of oxidative and radiative conditions, initial VOC and NO*x* concentrations, and temperature are explored with the model in section 3.3.

2. BOREAM Model Description

2.1. Atmospheric Sinks of α-Pinene

[6] Before describing the BOREAM model, we present a model estimation of the relative contributions of the oxidants O_3, OH and NO_3 to the overall sink of α-pinene in atmospheric conditions. The model used is the three-dimensional chemistry/transport model IMAGES [*Stavrakou and Müller*, 2006]. Since O_3, OH and NO_3 exhibit very distinct diurnal patterns in the atmosphere (with OH and NO_3 being mostly present during the day and during the night, respectively), the diurnal cycle of the emissions is of great significance in order to assess their role in the oxidation of the short-lived compound α-pinene. Diurnally varying emissions are calculated here using a detailed canopy environment model and meteorological fields obtained from ECMWF analyses, as described by *Müller et al.* [2007]. Although many past studies assumed that the emissions of terpenes are light-independent, and therefore nonzero at night, field studies have shown that terpene emissions by broadleaved plants follow a diurnal cycle similar to isoprene's, and that the light-independent emission algorithm is a special case thought to be valid only for coniferous trees [*Kesselmeier*, 2004; *Dindorf et al.*, 2006]. Monoterpene emissions are therefore estimated here using a light-independent algorithm [*Guenther et al.*, 1995] for coniferous trees, and the MEGAN isoprene algorithm [*Guenther et al.*, 2006] otherwise. On the basis of these assumptions, nighttime emissions represent less than 4% of

the global monoterpene source, and are negligible below the tropics.

[7] The chemical lifetime of α-pinene is calculated to range between less than half an hour, in the most polluted areas (northeastern China), to more than 5 hours at the most remote places (western Amazonia). This difference can be primarily attributed to NO_x emissions which enhance the abundance of OH and NO_3, and to a lesser extent ozone. The estimated relative contributions of OH and ozone to the sink of α-pinene are illustrated in Figure 1. The contribution of the nitrate radical exceeds 20% over Europe, the northeastern United States and eastern China, while it is less than 5% over equatorial and boreal forests. At the global scale, the reactions with OH, O_3 and NO_3 represent 42, 46 and 12% of the total sink of α-pinene, respectively. Ozone is calculated to be the main oxidant (>70%) over remote forests. The oversimplification of the α-pinene chemical mechanism in IMAGES might have a significant impact on these results, but it should be limited in most environments, since monoterpene emissions are generally dwarfed by isoprene's in most areas. However, the role of OH could be much larger than calculated here, if the findings of the recent GABRIEL campaign in Surinam are confirmed, since they indicate that OH levels might be strongly underestimated by current models, possibly because of deficiencies in the isoprene oxidation mechanism [*Kubistin et al.*, 2007].

2.2. Explicit Mechanism for the Formation of Primary Products

[8] The oxidation of α-pinene and pinonaldehyde by OH is based on the mechanism described by *Peeters et al.* [2001] and *Capouet et al.* [2004]. An important modification, illustrated in Figure 2, concerns the fate of a peroxy radical (6-OH-menthen-8-peroxyl, or R_7O_2 the work by *Capouet et al.* [2004, Figure 1]) formed after addition of OH to site *c* of α-pinene followed by ring-opening of the adduct and addition of O_2 in either anti or syn form with respect to the OH group, the first being estimated at 60% [*Peeters et al.*, 2001]. Besides the usual reactions of peroxy radicals, the anticase peroxy radical can undergo a 1,6-shift of the hydrogen from the OH group to produce a radical with a hydroperoxide functionality [*Vereecken et al.*, 2007]. Further reactions of this compound lead to stable compounds of masses 184 (a keto-hydroperoxide) and 200 (a keto-hydroxy-hydroperoxide). Compounds of such masses have been observed in α-pinene + OH experiments by *Aschmann et al.* [1998] using API-MS. Although these compounds were heretofore unidentified, their molar yields estimated at 19% and 11% by *Aschmann et al.* [1998] makes them major products. The rate for the 1,6-H-shift is taken to be 1000 s^{-1} in order to match the observations of *Aschmann et al.* [1998] at the laboratory conditions (8 ppm NO). A detailed discussion of this critical rate and of the subsequent reaction pathways is provided by *Vereecken et al.* [2007]. In atmospheric as well as in most laboratory conditions, this 1,6-H-shift is faster than ring closure and reaction with NO. Therefore the yields of by-products of the anticase of the oxy radical R_7O (e.g., HCA168 in the work by *Capouet et al.* [2004]) become negligible in most situations.

[9] The OH-initiated mechanism has been extended to encompass the oxidation by ozone and NO_3. The determination of the fate of alkoxy radicals relies on theoretical calculations of the barrier heights for each reaction of potential importance. Quantum chemical computations are based on DFT (density functional theory) calculations at the B3LYP-DFT/6-31G(d, p) level, in combination with statistical rate theories (Transition state theory and RRKM theory).

[10] The peroxy radical reactions are described by *Capouet et al.* [2004]. In particular, the characterization of the permutation reactions of peroxy radicals is based on an extensive review of literature data. The reactions of a peroxy radical with the other RO_2's are represented in the model as reactions with counter species for the different classes of peroxy radicals, each class being characterized by a typical self-reaction rate ranging between 10^{-16} cm^{-3} $molecule^{-1}$ s^{-1} and 1.5×10^{-11} cm^{-3} $molecule^{-1}$ s^{-1}. In this way, the total number of permutation reactions is kept limited, being equal to the number of peroxy radicals multiplied by the number of RO_2 classes (10).

[11] The general lines of the ozonolysis mechanism (down to the formation of stable products) are shown in Figure 3. Addition of O_3 to the C = C bond forms a primary ozonide which rapidly decomposes to two Criegee intermediates in equal amounts [*Ma et al.*, 2007]. RRKM calculations indicate that ~12% and 18% of Criegee I and II stabilize thermally, respectively. Reaction of the stabilized Criegee intermediates with water vapor produces pinonaldehyde, a product identified by several groups using various experimental setups [*Hakola et al.*, 1994; *Alvarado et al.*, 1998; *Ruppert et al.*, 1999; *Yu et al.*, 1999; *Baker et al.*, 2002]. Although occurrence of this reaction path has been confirmed experimentally by *Warscheid and Hoffmann* [2001], the pathways to pinonaldehyde are not yet fully understood since this group observed also this compound in ozonolysis experiments under dry conditions. In contrast, *Berndt et al.* [2003] have observed a decrease of pinonaldehyde with increasing water, while *Baker et al.* [2002] observed no effect of water on this product.

[12] Early experimental estimates of the molar yield of OH radicals range between 0.70 and 0.83 [*Paulson et al.*, 1998; *Chew and Atkinson*, 1998; *Rickard et al.*, 1999] suggesting that the hydroperoxide channel is dominant. In the case of the Criegee intermediate I, the transition state leading to OH elimination undergoes a 1,4-H shift of either the tertiary hydrogen atom on position *g* (channel Ia) or the 3 primary hydrogen atoms on position *a* (channel Ib). The former route is a concerted process where the hydrogen migration is accompanied by the formation of a π bond between the carbon radical at site *b* and the β carbon (site *g*) from which the H atom is abstracted. This last one switches from a sp^3 to a planar sp^2 hybridization which substantially increases the ring strain in the four-membered ring. Quantum chemical calculations show that because of this increase in ring strain, the bond strength between the tertiary hydrogen atom and the β carbon site is nearly identical to the dissociation energy of the primary hydrogen atoms of site *a*. The calculated barrier heights for H-shift are also nearly identical, within 0.3 kcal/mol, such that the rate of migration per hydrogen can be considered identical for each site; the branching ratio of 1:3 for channel Ia versus channel Ib is due to the larger number of available H atoms on site *a*.

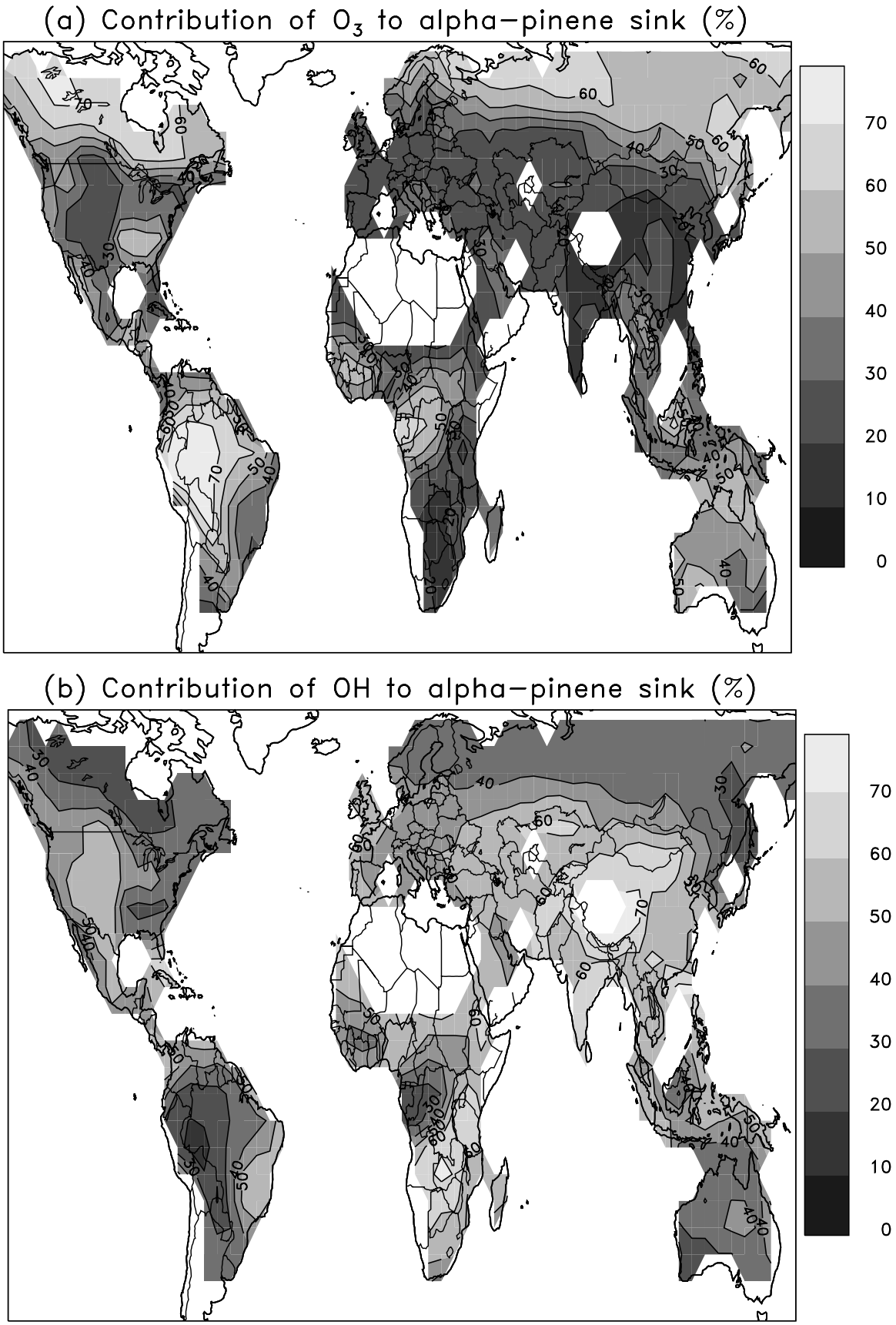

Figure 1. Relative contributions of (a) O_3 and (b) OH to the total (vertically integrated) sink of α-pinene calculated using the IMAGES model for the month of July.

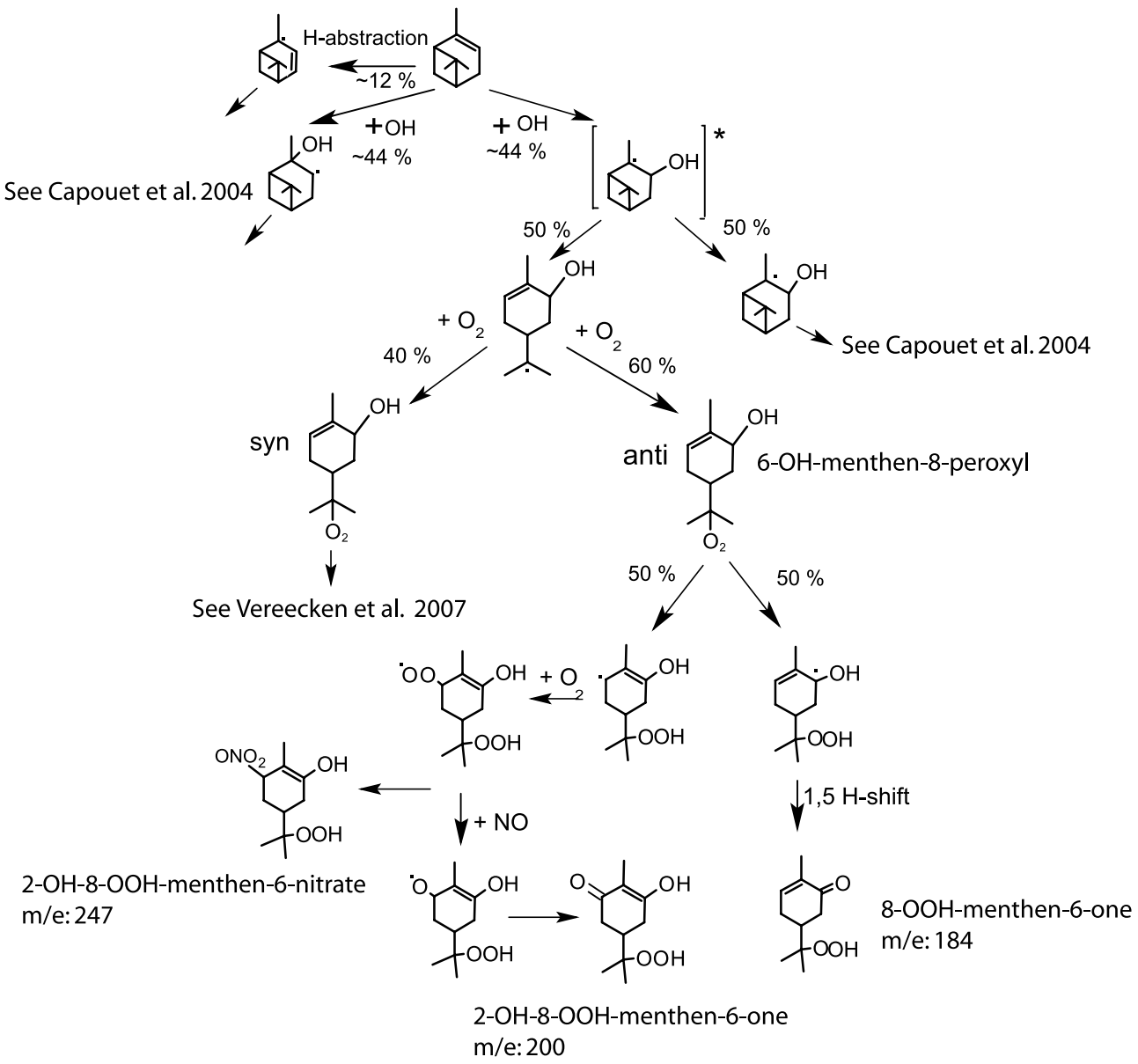

Figure 2. Pathway in the OH-initiated α-pinene oxidation mechanism leading to the formation of low-volatility hydroperoxides and involving the isomerization of the anticase 6-OH-menthen-8-peroxy radical.

[13] The channel Ia has been described in the study of *Fantechi et al.* [2002] related to the oxidation of pinonaldehyde. It is somewhat different from other mechanisms proposed in the literature. *Winterhalter et al.* [2003] proposed CH_3CO elimination from intermediate R_2O. Our calculations show that CH_3CO elimination requires at least 4 kcal/mol, while the breaking of the four-membered ring forming R_3 is essentially barrierless because of the higher exothermicity. The MCM mechanism [*Saunders et al.*, 2003] proposes acetone elimination from the oxy radical R_3O. However, the much higher barrier for this reaction, 7 kcal/mol above the H-shift, makes it a negligible process. Various mechanistic schemes have been also proposed for the oxidation chain of channel Ib. *Jenkin et al.* [2000] and *Saunders et al.* [2003] propose a 1,8-H shift isomerization for R_5O. Calculated barrier heights are 4.2 kcal/mol and 7.6 kcal/mol for the formaldehyde elimination and the hydrogen atom migration, respectively. Taking into account the frequency factor ratio of 250 ± 50 between these processes, the decomposition is about 3×10^4 faster than the hydrogen shift. 1,7 H-shift has been suggested for the next oxy radical R_6O [*Jenkin et al.*, 2000; *Saunders et al.*, 2003; *Winterhalter et al.*, 2003] to explain the formation of pinic acid. Quantum chemical calculations give a barrier height of 1.58 kcal/mol for the hydrogen shift versus a straight, barrierless CO_2 elimination. The 50 to 100 times higher frequency factor strengthen the dominance of the decomposition process. Acetone elimination from R_8O proposed by *Saunders et al.* [2003] is unlikely because of the calculated barrier difference of 7 kcal/mol with respect to the 1, 5-H shift, similarly to the case of R_3O of analogous structure. The alkyl radical R_7 resulting from the decompo-

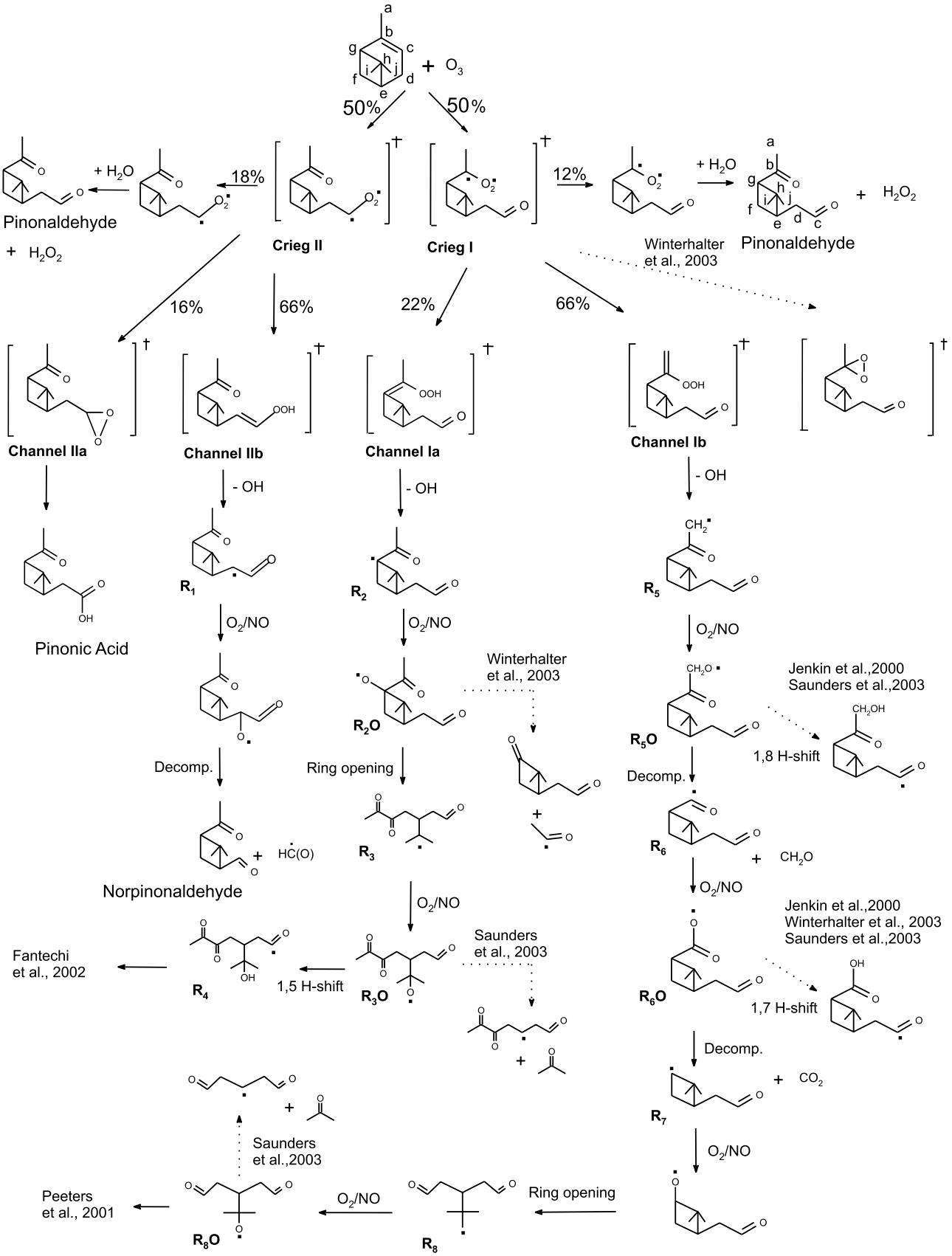

Figure 3. Main paths of the α-pinene oxidation by O_3 (in presence of NO). Alternative routes proposed in the literature are represented by the dotted arrows.

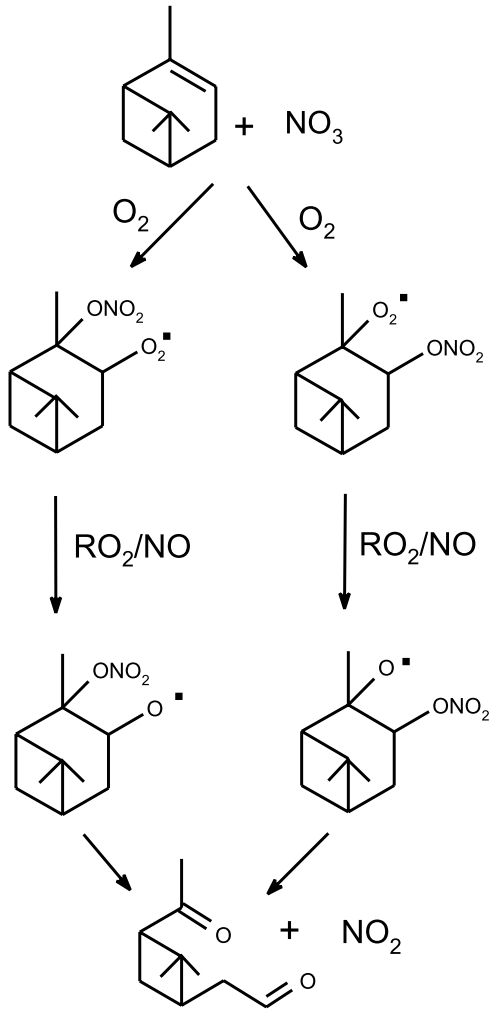

Figure 4. Main paths of the α-pinene oxidation by NO_3.

sition is also formed in the OH oxidation detailed by *Peeters et al.* [2001].

[14] The ester channel (IIa) of Criegee intermediate II competes with the hydroperoxide channel (IIb). Whitten-Rabinovitch RRKM calculations give a branching ratio IIb/IIa = 4 ± 2. The ester channel rapidly forms pinonic acid, a well-known product observed in α-pinene ozonolysis experiments [*Hatakeyama et al.*, 1991; *Hoffmann et al.*, 1997; *Christoffersen et al.*, 1998; *Jang and Kamens*, 1999; *Yu et al.*, 1999; *Glasius et al.*, 2000; *Koch et al.*, 2000]. The fate of radical R_1 resulting in HCO elimination has been already described in the study of *Fantechi et al.* [2002] related to the pinonaldehyde oxidation. The 1, 2-H shift proposed in the MCM mechanism for the activated radical, precursor of R_1 is calculated to be about 10^4 times slower than collisional stabilization.

[15] Since the ozonolysis mechanism described above strongly underestimates the yields of low-volatility organic acids which have been observed in significant amounts in the aerosol formed in α-pinene ozonolysis experiments [e.g., *Yu et al.*, 1999; *Glasius et al.*, 2000; *Koch et al.*, 2000; *Winterhalter et al.*, 2003; *Presto et al.*, 2005a], the model results will be presented in section 3.3 for both the standard mechanism and a modified version, where pinic acid, hydroxy pinonic and pinalic acid are produced directly from the first Criegee Intermediate (Crieg I in Figure 3) [*Ma et al.*, 2007], with assumed overall yields from α-pinene ozonolysis of 5%, 3% and 3%, respectively, based on the total (gas + particle) yields measured by *Yu et al.* [1999]. The other reaction channels of Crieg I are scaled down accordingly. The results obtained with this modified mechanism should, at best, be considered as indicative, since the precise pathways leading to these acids, and therefore also the dependence of their yields on photochemical conditions are currently unknown.

[16] Oxidation of α-pinene by NO_3 is minor but non-negligible in the smog chamber experiments simulated in section 5. The two main NO_3 addition routes lead to the formation of pinonaldehyde, as proposed by *Wängberg et al.* [1997] and depicted in Figure 4. Box model simulations of α-pinene + NO_3 laboratory experiments performed in the absence of NO [*Hallquist et al.*, 1999] yield 70% pinonaldehyde and 20% organic nitrates, in agreement with the measurements.

2.3. Chemistry of the First-Generation Products

[17] As mentioned above, a fully explicit mechanism for the oxidation of α-pinene should include $\gg 10^6$ reactions. The explicit mechanism described above represents only a tiny fraction of this large number which concerns primarily the further oxidation of the first generation products. Since the further oxidation of the first-generation products is expected to have a significant impact, even on the relatively short timescale of laboratory experiments (typically a few hours), protocols have been developed to represent these reactions. They are based on the methodology discussed by *Capouet et al.* [2004], with further developments described below. Pinonaldehyde being a major product, its gas phase oxidation and photodissociation are described in detail, following *Fantechi et al.* [2002] and *Capouet et al.* [2004].

[18] The OH oxidation rates of the products for which no data are available have been estimated on the basis of the structure-activity relationships (SARs) elaborated by *Neeb* [2000], with a number of modifications described below.

[19] Theoretical investigations by *Vereecken and Peeters* [2002] on pinonaldehyde, pinic acid, pinonic acid and related compounds show that the four-membered ring induces structural effects (e.g., ring strain and strain-enhanced hyperconjugation stabilization) which affect the C-H bond strengths and therefore the H abstraction rates. In particular, the rate constant for abstraction at site *d* (see, e.g., pinonaldehyde in Figure 3) is significantly affected by the presence of the ring and the nature of the chemical groups connected to its ends. For example, an aldehyde group at site *d* increases the rate several times more than a carboxylic group. On the basis of these theoretical results, a simple SAR has been deduced for H abstraction at site *d* for compounds with a four-membered ring connected to oxygenated groups involving an sp^2 carbon. The different types of structures considered are summarized in Figure 5. The influence of additional functional groups (-ONO_2 at site *d* or *e*, -OH at site *d*) follows the SAR of *Neeb* [2000].

Carbon structure	Rate (10^{-11} cm^3 molec.$^{-1}$s^{-1})	Reference compound
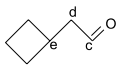	8.1	1,1-di-me-2-$CH_2CH(O)$-cyclobutane pinonaldehyde
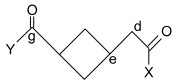	4.1	pinonic acid
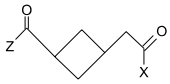	2.5	pinic acid

X denotes an alkyl, -OH or -O_2NO_2 group
Y denotes an alkyl group or an H atom
Z denotes a -OH or -O_2NO_2 group

Figure 5. SAR for H abstraction rate at site *d* of α-pinene oxidation products bearing a cyclobutyl ring.

[20] On the basis of recent experimental data reported by *Atkinson et al.* [2005] and *Schurath and Naumann* [2003, and references therein], the abstraction rates are set to 16.9×10^{-12} cm^{3}molecule^{-1}s^{-1} for an aldehydic hydrogen, and 3.5×10^{-12} cm^{3}molecule^{-1}s^{-1}for a tertiary hydrogen adjacent to a ketone. The rate recommended by *Atkinson et al.* [2005] for the reaction of NO_3 with pinonaldehyde is used for all $C_{\geq 7}$ aldehydes. Addition of O_3 on double bonded products is assumed to occur at the same rate as for α-pinene. The impact of these reactions is minor in the model simulations.

[21] The photolysis rates are computed using a photolysis calculation package based on the TUV model [*Madronich and Flocke*, 1998]. Photodissociation is considered for the following chromophores: aldehyde, ketone, hydroperoxide, alkyl nitrate, and peroxy acyl nitrate. Given the lack of direct experimental data for the photodissociation of a large majority of products in our mechanism, the photolysis parameters are estimated on the basis of reference compounds of similar structure for which photolysis data are available (Table 1). In

Table 1. Photolysis Channels Considered in This Study and Reference Compounds for the Estimation of the Photolysis Parameters

Compound Structure	Channel	Reference Compound
$-CH_2-CH_2-CH_2-CH(O)$[a]	$\rightarrow -CH_2=CH_2+CH_3CH(O)$	C_{4-7} *n*-aldehydes
$-CH_2-CH_2-CH_2-CH(O)$	$\rightarrow -CH_2-CH_2-CH_2\cdot+\cdot CHO$	
$-CRR'-CH(O)$[b,c]	$\rightarrow -CRR'H+CO$	iso-butyraldehyde
$-CRR'-CH(O)$	$\rightarrow -CRR'\cdot+\cdot CHO$	
$R-C(O)-R'$[d,e]	$\rightarrow R-C(O)\cdot+R'\cdot$	methyl-ethyl-ketone
$R-C(O)-R'$	$\rightarrow R'-C(O)\cdot+R\cdot$	
$>C=CR-CH(O)$[c,f,g]	$\rightarrow >C=CRH+CO$	acrolein, methacrolein
$>C=CR-CH(O)$	$\rightarrow >C=CR\cdot+\cdot CHO$	
$>C=CR-CH(O)$	$\rightarrow >C=CR-C(O)\cdot+H$	
$R-C(O)CR'=C<$[g,f]	$\rightarrow R-CR'=C<+CO$	methyl vinyl ketone
$R-C(O)CR'=C<$	$\rightarrow \cdot CR'=C<+R-C(O)\cdot$	
$R-C(O)CR'=C<$	$\rightarrow R\cdot+\cdot C(O)CR'=C<$	
$-C(O)CH(O)$	$\rightarrow -C(O)\cdot+HO_2+CO$	methyl glyoxal
$-COHCH(O)$[g]	$\rightarrow -COH\cdot+HO_2+CO$	glycoaldehyde
$-COHCH(O)$	$\rightarrow -CHOH+CO$	
$R-C(O)-COH<$[g]	$\rightarrow R-C(O)\cdot+\cdot COH<$	hydroxyacetone
$R-C(O)-COH<$	$\rightarrow R\cdot+\cdot C(O)-COH<$	hydroxyacetone
$RONO_2$[h]	$\rightarrow RO\cdot+NO_2$	2-butyl nitrate
$-C(O)-CRR'ONO2$[i]	$\rightarrow -C(O)CRR'O\cdot+NO_2$	3-nitrooxy-2-butanone
$-C(O)-CRR'ONO2$	$\rightarrow -C(O)\cdot+\cdot CRR'ONO_2$	
$-C(O)O_2NO_2$	$\rightarrow -C(O)O_2\cdot+NO_2$	
$-C(O)O_2NO_2$[g]	$\rightarrow -C(O)O\cdot+NO_3$	peroxypropionyl nitrate
$R-OOH$[h]	$\rightarrow RO.+OH$	methyl hydroperoxide
$R-C(O)-R'-CH(O)$[e,j]	$\rightarrow R-C(O)\cdot+\cdot R'-CH(O)$	pinonaldehyde
$R-C(O)-R'-CH(O)$[j]	$\rightarrow R\cdot+\cdot C(O)R'-CH(O)$	
$R-C(O)-R'-CH(O)$	$\rightarrow R-C(O)-R'\cdot+\cdot CHO$	
$R-C(O)-R'-CH(O)$[k]	$\rightarrow$ molecular channel	

[a] *Atkinson et al.* [2005], *Tadic et al.* [2001a, 2001b, 2002].
[b] *Desai et al.* [1986].
[c] R may also be an hydrogen atom.
[d] Quantum yield taken equal to the quantum yield of acetone multiplied by 1.2 in order to match the averaged yield measured by *Raber and Moortgat* [1995].
[e] The release of CH_3CO is the only path considered when R is a methyl group. Both channels are of equal importance in the other cases.
[f] The molecular channel accounts for 60%, while the two minor channels are in the same ratio.
[g] *Sander et al.* [2006].
[h] *Atkinson et al.* [2005].
[i] Quantum yield assumed to be unity. The ratio of the nitrate and ketone photolysis quantum yields is taken equal to the ratio of the quantum yields for the photodissociation of methyl ethyl ketone and 2-butyl nitrate. The resulting photodissociation of the ketone functionality is small (15%) even in the UV spectrum, as suggested by *Barnes et al.* [1993]. R and R' may also be hydrogen atoms.
[j] *Capouet et al.* [2004].
[k] Channel producing only stable molecules. Represented by the molecular channels of C_{3-7} *n*-aldehydes, iso-butyraldehyde or pinonaldehyde (when R' is a four-membered cycle).

general, each functionality is treated independently in a multifunctional compound. Exceptions to this rule are the cases of hydroxy carbonyls, keto-nitrates and keto-aldehydes, when the functionalities are located on neighboring carbons, and the case of $C_{\geq 7}$ keto-aldehydes, which are treated like pinonaldehyde, as described by *Capouet et al.* [2004].

[22] Alkyl radicals are assumed to react promptly with oxygen, generating peroxy radicals, except for the following substituted structures where either decomposition or reaction with O_2 leads to the formation of a stable product [*Saunders et al.*, 2003; *Vereecken et al.*, 2004; *Hermans et al.*, 2005]:

$$\mathrm{RCH \cdot OOH \rightarrow RCH(O) + OH} \quad (1)$$

$$\mathrm{RCH \cdot OH + O_2 \rightarrow RCH(O) + HO_2} \quad (2)$$

$$\mathrm{RCH \cdot ONO_2 \rightarrow RCH(O) + NO_2} \quad (3)$$

$$\mathrm{RR'C \cdot OOH \rightarrow RR'C(O) + OH} \quad (4)$$

$$\mathrm{RR'C \cdot OH + O_2 \rightarrow RR'C(O) + HO_2} \quad (5)$$

$$\mathrm{RR'C \cdot ONO_2 \rightarrow RR'C(O) + NO_2} \quad (6)$$

[23] In order to simplify the overall oxidation mechanism, the species formed from the oxidation of minor products (i.e., of yield <5%) are crudely lumped together into generic peroxy radicals and/or acyl peroxy radicals. The generic peroxy radicals are either short-chained (SXO_2) or long-chained ($LXaO_2$, $LXbO_2$, $LXcO_2$, $LXdO_2$). Their chemistry follows the lines described by *Capouet et al.* [2004]. The third letter in the LX compounds (a, b, c or d) correspond to volatility classes of the stable products formed from their reactions, as further discussed in section 5. The acyl peroxy radicals follow the same classification, with SXO_3 as the short-chained radicals and $LXaO_3$ to $LXdO_3$ as the long-chained acyl peroxy radicals.

[24] The compounds formed in the oxidation of major products (yield >5%) are lumped according to their carbon number and oxygenated functionalities. This procedure neglects the fine molecular structure but keeps the essential structural information needed to estimate the chemical loss rates and the vapor pressures of the stable products formed through this "semigeneric" chemistry. In order to illustrate this methodology, consider the reactions of the peroxy radicals R_1O_2, R_2O_2 and R_5O_2 (see Figure 3) with HO_2, forming hydroperoxides with two carbonyl functionalities. The reactivity and volatility of their oxidation products are generally similar, and they can therefore be lumped together. A subset of the oxidation mechanism of R_5OOH is shown in Table 2. Because of the loss of information caused by the lumping, the fate of semigeneric alkoxy radicals cannot be characterized. Their subsequent chemistry is therefore not represented in the mechanism, except in the following cases for which we assume that only one oxidation channel occurs:

$$\mathrm{RCHO \cdot CH_2OH \rightarrow RCH(O) + \cdot CH_2OH} \quad (7)$$

$$\mathrm{RR'CO \cdot CH_2OH \rightarrow RR'C(O) + \cdot CH_2OH} \quad (8)$$

$$\mathrm{RCHO \cdot CH(O) \rightarrow RCH(O) + \cdot CHO} \quad (9)$$

$$\mathrm{RCHO \cdot CH_2OOH \rightarrow RCH(O) + \cdot CH_2OOH} \quad (10)$$

$$\mathrm{RCHO \cdot CH_2ONO2 \rightarrow RCH(O) + \cdot CH_2(O)NO_2} \quad (11)$$

$$\mathrm{RR'CO \cdot CH_2ONO2 \rightarrow RR'C(O) + \cdot CH_2(O)NO_2} \quad (12)$$

$$\mathrm{RC(O)C(O)\cdot \rightarrow RC(O) \cdot + CO} \quad (13)$$

$$\mathrm{RC(O)O\cdot \rightarrow R \cdot + CO_2} \quad (14)$$

This applies, for example, to the acyl-oxy radical L10KPC(O)O (reaction (R16) in Table 2). In the other cases (e.g., for L9KPO), however, the further chemistry is ignored at this stage. As shown by this example, when the fate of a semigeneric or generic compound cannot be deduced with some confidence, it is, depending on its size, converted to SX_LOST (<7 carbon atoms) or LX_LOST ($\geq$7 carbon atoms) and is thereby effectively removed from the model. Consequently, mass conservation does not hold in our model. An alternative way of treating the unknown chemistry of generic and semigeneric products could be to treat the compounds SX_LOST and LX_LOST as either some combination of generic peroxy radicals, or as stable molecular compounds undergoing further OH reactions and photolyses and generating generic peroxy radicals. Such parameterization could be developed in the future, on the basis of the observed temporal evolution of gaseous and SOA concentrations from laboratory measurements, after consumption of α-pinene. At present, however, the existing data sets are too limited for that purpose.

2.4. Kinetic Aerosol Model

[25] The partitioning of a compound i between the gas and particulate phases is governed by an equilibrium constant $K_{p,i}$ (μg^{-1} m^3) [*Pankow*, 1994a, 1994b] defined by

$$C_{p,i}/C_{g,i} = K_{p,i} \cdot [M_o] \quad (15)$$

where $C_{p,i}$ and $C_{g,i}$ are the particulate and gas phase concentrations of compound i, and $[M_o]$ is the aerosol concentration (in μg m^{-3}). The partitioning coefficient can be expressed in terms of thermodynamical properties:

$$K_{p,i} = \frac{760 \cdot RT \cdot f_{om}}{MW_{om} \cdot 10^6 \cdot \zeta_i \cdot p^0_{L,i}}, \quad (16)$$

Table 2. Reaction Mechanism (Subset) of $CH(O)CH_2GC(O)CH_2OOH$ (or R_5OOH, see Figure 3)[a]

Reaction No.	Reaction	Rate
(R1)[b]	$R_5OOH + OH \rightarrow L10KPC(O)O2$	16.9×10^{-12}
(R2)[c]	$R_5OOH + OH \rightarrow CH(O)CH2GC(O)CH(O) + OH$	5.3×10^{-12}
(R3)[d]	$R_5OOH + OH \rightarrow L10KLPO2$	12.5×10^{-12}
(R4)	$R_5OOH + NO_3 \rightarrow L10KPC(O)O2 + HNO_3$	$1.7 \times 10^{-12} \times e^{-1490/T}$
(R5)	$R_5OOH + h\nu \rightarrow CH(O)CH_2GC(O)CH_2O + OH$	J(ROOH)
(R6)	$R_5OOH + h\nu \rightarrow CH(O)CH_2G + C(O)CH_2OOH$ $R_5OOH + h\nu \rightarrow CH(O)CH_2GC(O) + CH_2OOH$	$0.5 \times J_1(R - C(O) - R' - C(O)H)$ $0.5 \times J_1(R - C(O) - R' - C(O)H)$
(R7)	$R_5OOH + h\nu \rightarrow SXKET + SXCH(O)$	$J_2(R - C(O) - R' - C(O)H)$
(R8)	$L10KPC(O)O2 + NO \rightarrow L10KPC(O)O + NO_2$	$J_3(R - C(O) - R' - C(O)H)$
(R9)	$L10KPC(O)O2 + NO \rightarrow L10KPC(O)O + NO_2$	$1.7 \times 10^{-12} e^{-1460/T}$
(R10)	$L10KPC(O)O2 + NO_2 \rightarrow L10KMP$	$1.1 \times 10^{-11} \times (300/T)$
(R11)	$L10KPC(O)O2 + NO_3 \rightarrow L10KPC(O)O + NO_2$	4.1×10^{-12}
(R12)	$L10KPC(O)O2 + HO_2 \rightarrow L10AKP + O_3$	$0.29 \times 4.3 \times 10^{-13} e^{1040/T}$
(R13)	$L10KPC(O)O2 + HO_2 \rightarrow L10AKP + O_2$	$0.71 \times 4.3 \times 10^{-13} e^{1040/T}$
(R14)[e]	$L10KPC(O)O2 + RO_2 \rightarrow \alpha L10KPC(O)O + \beta L10AKP$	
(R15)	$L10KPC(O)O + O2 \rightarrow L9KPO2 + CO_2$	prompt
(R16)	$L9KPO2 + NO \rightarrow L9KNP$	$0.26 \times 2.5 \times 10^{-12} e^{360/T}$
(R17)	$L9KPO2 + NO \rightarrow L9KPO + NO_2$	$0.26 \times 2.5 \times 10^{-12} e^{360/T}$
(R18)	$L9KPO2 + NO_3 \rightarrow L9KPO + NO_2$	2.3×10^{-12}
(R19)	$L9KPO2 + HO_2 \rightarrow L9KPP + O_2$	$2.9 \times 10^{-12} e^{1250/T}$
(R20)[e]	$L9KPO2 + RO_2 \rightarrow \alpha L9KPO + \beta L9KKP + \gamma L9HKP$	
(R21)	$L9KPO \rightarrow LX\_LOST$	prompt
(R22)	$L10KMP \rightarrow L10KPC(O)O2 + NO_2$	$2.8 \times 10^{16} e^{-13580/T}$
(R23)[f]	$L10KMP + OH \rightarrow OH + L10KKM$	5.3×10^{-12}
(R24)[g]	$L10KMP + OH \rightarrow LXdO2$	4.1×10^{-12}
(R25)[h]	$L10KMP + OH \rightarrow LXdO2$	4.0×10^{-12}
(R26)	$L10KMP + h\nu \rightarrow SXO3 + LXcO2$	$J(R - C(O) - R')$
(R27)	$L10KMP + h\nu \rightarrow NO_2 + L10KPC(O)O2$	$0.8 \times J(- C(O)O_2NO_2)$
(R28)	$L10KMP + h\nu \rightarrow NO_3 + L10KPC(O)O$	$0.2 \times J(- C(O)O_2NO_2)$
(R29)	$L10KMP + h\nu \rightarrow OH$	J(ROOH)

[a]"G" denotes a dimethyl-cyclobutyl ring. The prefix L followed by the carbon number denotes semigeneric species. The next characters identify the chemical functionalities: A, carboxylic (per)acid; H, hydroxy; K, ketone; L, aldehyde; M, peroxy acyl nitrate; N, organic nitrate; P, hydroperoxide. Compounds prefixed by LX or SX are $C_{\geq 7}$ and $C_{<7}$ generic compounds, respectively.

[b]Abstraction at site *c* (see Figure 2 for the identification of the sites).

[c]Abstraction at site *a* (see Figure 2 for the identification of the sites).

[d]Channel grouping H abstraction reactions at sites *d*, *e*, *f*, *g*, *i* and *j* (same labeling as for pinonaldehyde in Figure 2).

[e]The rates and stoichiometric coefficients depend on the RO_2 class [*Capouet et al.*, 2004]. Semigeneric radicals are assumed to react like secondary alkyl peroxy radicals.

[f]H abstraction rate for a C atom single-bonded to an O in a semigeneric compound. The hydroperoxide functionality is assumed to decompose to a carbonyl, according to equation (1).

[g]H abstraction rate for a C atom adjacent to a ketone C in a semigeneric compound.

[h]H abstraction rate for the other carbons of a C_{10} compound.

where R is the gas constant (atm m^3 K^{-1} mol^{-1}); T is temperature (K); MW_{om} is the molecular weight of the absorbing medium (g mol^{-1}); f_{om} is the weight fraction of organic matter in the total aerosol; ζ_i is the activity coefficient of compound i in the particulate phase; $p^0_{L,i}$ is its subcooled vapor pressure (here in Torr); 760 (Torr atm^{-1}) and 10^6 (μg g^{-1}) are unit conversion factors. We adopt the kinetic representation of the partitioning proposed by *Kamens et al.* [1999]:

$$K_{p,i} = \frac{k_{on,i} \cdot N_{Avo}}{MW_{om} \cdot 10^{12} \cdot k_{off,i}} \quad (17)$$

where $k_{on,i}$ and $k_{off,i}$ are the adsorption (molecule^{-1} cm^3 s^{-1}) and desorption (s^{-1}) rates, respectively, and $N_{Avo} = 6.023 \times 10^{23}$ molecules mol^{-1}. Adsorption and desorption of a compound X are implemented as chemical reactions in the model:

$$k_{on,i} : X + OA \rightarrow X_p + OA + OA \quad (18)$$

$$k_{off,i} : X_p \rightarrow X - OA \quad (19)$$

where OA is a counter species representing the total organic aerosol, and X and X_p represent the compound X in the gaseous and particulate phases, respectively.

[26] The adsorption rate of a gas by a particle is parameterized as [*Lelieveld and Crutzen*, 1991]:

$$k_{on} = \frac{MW_{om}}{\rho N_{Avo}} \cdot \left(\frac{a^2}{3D_g} + \frac{4a}{3\omega\gamma} \right)^{-1}, \quad (20)$$

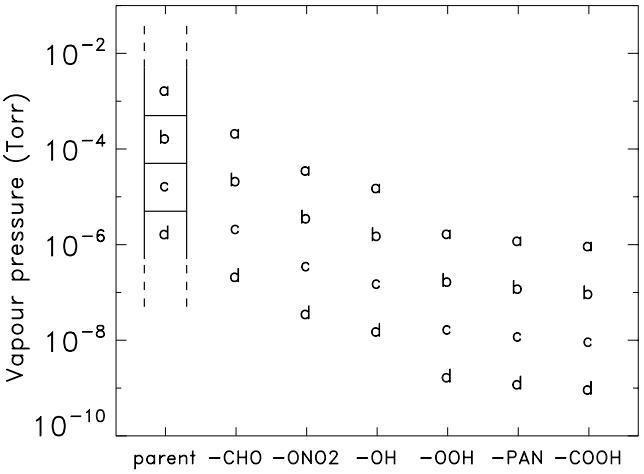

Figure 6. Vapor pressure of the generic products (prefixed by "LX") at 298 K, depending on the functionality (see abscissa) and the volatility class (denoted by a, b, c and d). The volatility classes are defined by the vapor pressure of the parent compound, as indicated by the vapor pressure ranges on the left.

where ρ is the aerosol density (g cm^{-3}); a is the particle radius (cm^2); D_g, the diffusivity in the gas phase [*Fuller et al.*, 1969]; ω is the mean gas phase molecular speed (cm s^{-1}) and γ is the accommodation coefficient (dimensionless). To the best of our knowledge, there is no experimental data for the accommodation coefficients of organic species on organic aerosols. Here, we assume γ equal to 0.2 for all compounds, on the basis of the value deduced by [*Bowman et al.*, 1997] from simulations of smog chamber experiments of m-xylene photo-oxidation. The aerosol size is estimated from the assumption of a unique, spherical size bin and a constant particle number. The results shown in the next section show very little dependence on the number and initial diameter of the seed particles.

[27] The desorption rate $k_{off,i}$ is obtained from equations (16), (17) and (20). It is generally assumed that the activity coefficient of organics in organic aerosol particles is close to one [*Kamens et al.*, 1999]. MW_{om} is calculated at each time step in the model, on the basis of the molecular masses of the particulate products. The vapor pressure of the chemical compounds generated by the oxidation of terpenes range from 10^{-2} to 10^{-7} Torr [*Hallquist et al.*, 1997; *Hoffmann et al.*, 1997; *Bilde and Pandis*, 2001]. We use the group contribution method of *Capouet and Müller* [2006] which expresses the vapor pressure of a compound i as

$$\log_{10}\left(p^0_{L,i}\right) = \log_{10}\left(p^0_{L,parent}\right) + \sum_k \nu_{k,i}\cdot\tau_k \qquad (21)$$

where $p^0_{L,parent}$ is the vapor pressure of the parent compound, i.e., the compound i with its oxygenated functionalities replaced by H atoms, $\nu_{k,i}$ is the number of functionalities of type k in compound i, and τ_k are the temperature-dependent group contribution parameters provided by *Capouet and Müller* [2006]. As explained in the previous section, generic $C_{\geq 7}$ peroxy radicals (prefixed by "LX") are formed in the oxidation of either explicit or semigeneric compounds. The vapor pressure of the parent compound at 298 K ($p^0_{L,parent}$) determines the volatility class of the generic peroxy radical:

$$\text{LXa} : p^0_{L,parent} \geq 5\cdot 10^{-4}\ \text{Torr} \qquad (22)$$

$$\text{LXb} : 5\cdot 10^{-4}\ \text{Torr} > p^0_{L,parent} \geq 5\cdot 10^{-5}\ \text{Torr} \qquad (23)$$

$$\text{LXc} : 5\cdot 10^{-5}\ \text{Torr} > p^0_{L,parent} \geq 5\cdot 10^{-6}\ \text{Torr} \qquad (24)$$

$$\text{LXd} : 5\cdot 10^{-6}\ \text{Torr} \geq p^0_{L,parent} \qquad (25)$$

The vapor pressures of compounds (e.g., LXbCHO) produced from the further reactions of the generic peroxy radicals are calculated using expressions similar to equation (21), where

$$\log_{10}\left(p^0_{L,parent}\right) = -2.8 - j + 0.035\cdot(T - 298) \qquad (26)$$

where j = 0, 1, 2 and 3 for LXa, LXb, LXc and LXd compounds, respectively. The temperature dependence has been determined from the averaged temperature dependence of the parent compounds replaced by the generic compounds. For example, the H abstraction reaction of L10KMP ($p^0_{L,parent} = 3.9\times 10^{-7}$ Torr at 298 K) generates a radical LXdO2 (reaction (R24) of Table 2). Its reaction with NO forms an organic nitrate LXdONO2 of lower p^0_L due to the additional nitrate functionality. Figure 6 shows both the vapor pressure ranges which define the volatility classes and the vapor pressures of the generic products at 298 K.

2.5. Particle Phase Reactions of Aldehydes and Hydroperoxides

[28] The acid-catalyzed, surface reaction of gas phase aldehydes with particle phase hydroperoxides hypothesized by *Tobias and Ziemann* [2000] is not considered here. On the other hand, peroxyhemiacetals have been observed to be formed reversibly from the reaction of aldehydes with hydroperoxides in the liquid phase [*Antonovskii and Terent'ev*, 1967],

$$\text{ROOH} + \text{R}'\text{CHO} \rightarrow \text{ROOC(OH)R}'\text{H} \qquad (27)$$

$$\text{ROOC(OH)R}'\text{H} \rightarrow \text{ROOH} + \text{R}'\text{CHO} \qquad (28)$$

The reactions of acetaldehyde, butyraldehyde and crotonaldehyde with 5 hydroperoxides in various solvents have been investigated experimentally by *Antonovskii and Terent'ev* [1967]. The association reaction rate was found to be strongly dependent on the dielectric permeability of the solvent, from values of about 0.01–0.02 M^{-1} s^{-1} at 20 C in a nonpolar solvent (CCl_4) to 10^{-3} M^{-1} s^{-1} in a mixture of $CHCl_3$ and hexanol. The dissociation rate of the peroxyhemiacetal also decreases several-fold in the most polar solvent, to about 10^{-4} s^{-1}, compared to its value in CCl_4. Activation energies of about 8 kcal/mole for the forward

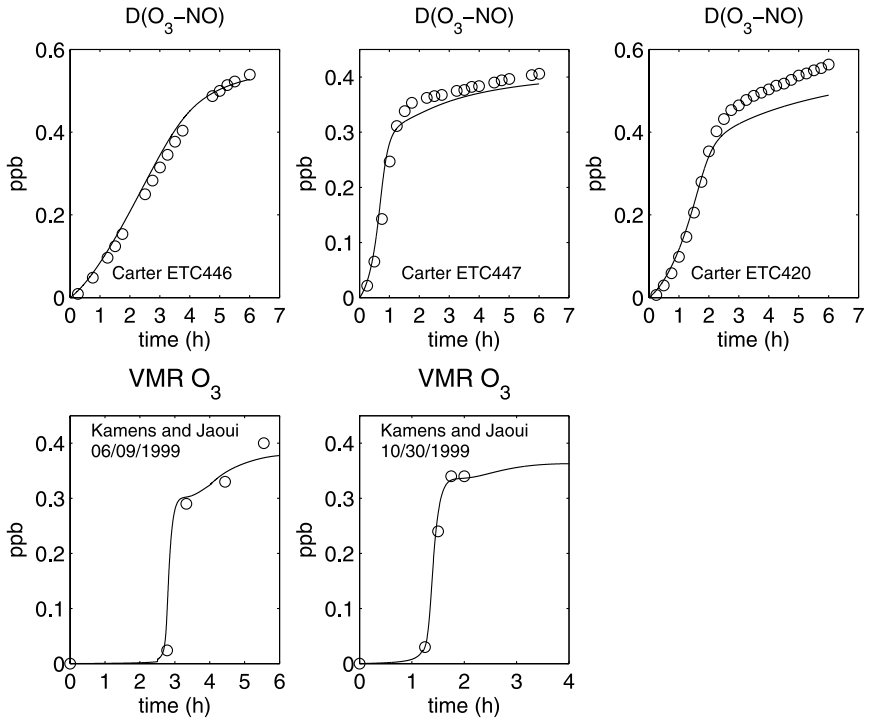

Figure 7. Time-dependent observed (circles) versus simulated (curves) $D(O_3-NO)$ (ppbv) for the α-pinene/NOx experiments of *Carter* [2000] and observed versus simulated O_3 mixing ratios (ppbv) in the experiments of *Kamens and Jaoui* [2001].

reaction in polar solvents and of about 10 kcal/mole for the backward reaction are deduced from the experiments at 20 and 40 C. In a similar study conducted by T. Tran and P. Ziemann at the University of California (P. Ziemann, personal communication, 2007), the association of acetaldehyde and heptaldehyde with cumene hydroperoxide and pernonanoic acid was investigated in two solvents (CCl_4 and CH_3CN), with results consistent with those of *Antonovskii and Terent'ev* [1967]. In particular, the rate constants for the reactions of heptaldehyde with the hydroperoxide and the peroxy acid were estimated to be 5×10^{-4} and 1.2×10^{-3} M^{-1} s^{-1} in CH_3CN. The association of the peroxy acid with heptaldehyde produced a compound which was observed to decompose into two organic acids, whereas an equilibrium was reached between equations (27) and (28) in the case of cumene hydroperoxide reacting with aldehydes.

[29] We test the influence of peroxyhemiacetal formation on SOA formation in the next section, by including model simulations obtained with association reactions of the 38 aldheydes and 37 hydroperoxides found to be the most abundant in the particle phase in the experiments described in section 3.2. The forward (k_{fwd}) and backward (k_{bck}) reaction rates used in these simulations are

$$k_{fwd} = 42500 \cdot \exp(-4000/T) \quad \left[M^{-1}s^{-1}\right] \tag{29}$$

$$k_{bck} = 2600 \cdot \exp(-5000/T) \quad \left[s^{-1}\right] \tag{30}$$

on the basis of the experimental results obtained in the most polar solvents. The equilibrium constant implied by these rates should be considered as an upper limit in the very polar SOA from α-pinene experiments. On the other hand, catalysis by the carboxylic acids present in SOA could enhance both the forward and backward reaction rates, but without affecting the equilibrium constant. Since the time needed to reach equilibrium is of the same order as the duration of the laboratory experiments considered in our study, this acid-catalysis should have a limited impact on the results.

3. Simulations of Chamber Experiments

3.1. Validation of the Model for Ozone Formation

[30] Before presenting the model confrontation with SOA measurements, we check the model performance for ozone formation. Note that the OH-initiated oxidation mechanism has already been validated for several gaseous compounds (NO, NO_2, pinonaldehyde, PAN-like compounds, organic nitrates) against laboratory data given by *Capouet et al.* [2004]. As described by *Carter and Lurmann* [1991], the quantity $D(O_3 - NO)$, defined as $([O_3]_t - [NO]_t) - ([O_3]_0 - [NO]_0)$, $[X]_t$ denoting the concentration of species X at time t, is a good indicator for the performance of the model regarding ozone formation. This quantity is displayed in Figure 7 as a function of time for both the model and the observations in the photo-oxidation experiments conducted in the SAPRC (Statewide Air Pollution Research Center) chambers [*Carter*, 2000]. These experiments used blacklights and initial α-pinene to NOx ratios varying approximately between 0.5 and 2. Figure 7 also shows the measured and simulated ozone mixing ratios in the experiments conducted by *Kamens and Jaoui* [2001] (see next

Table 3. Chamber Experiments Simulated in This Work[a]

Experiment	Reference	$\Delta\alpha$-pinene, ppb	$\Delta\alpha$-pinene/NOx	T, K	J(NO_2), 10^{-4} s^{-1}	Mo, $\mu g\ m^{-3}$	Y_{exp}, %	Y_A, %	Y_B, %
1	*Nozière et al.* [1999]	305	0.09	298	3.5	83	4.9	8.3	8.3
2		330	0.09	298	3.5	112	6.1	11.7	11.7
3		900	0.25	298	3.5	800	16.0	17.0	17.0
4		1500	0.52	298	3.5	2770	33.2	33.0	33.1
5	*Kamens and Jaoui* [2001]	940	1.9	300–308	30–44 (sun)	1180	22.3	18.6	20.7
6		980	2.2	295–315	12–34 (sun)	1092	21.5	17.0	19.7
7	*Hoffmann et al.* [1997]	19.5	0.17	309–315	83 (sun)	1.3	1.2	2.5	3.0
8		53	0.26	316–324	83 (sun)	8	2.7	0.6	0.7
9		72	0.35	309–315	83 (sun)	22.7	5.7	2.2	2.8
10		87.4	0.70	316–321	83 (sun)	38.2	7.9	1.3	1.6
11		94.5	0.70	316–321	83 (sun)	33	6.3	1.2	1.5
12		94.6	0.78	314–316	83 (sun)	34.2	6.5	2.2	2.7
13		95.5	0.77	314–316	83 (sun)	39.3	7.4	2.2	2.7
14	*Takekawa et al.* [2003]	45	1.8	283	40	52.1	20.8	18.8	21.4
15		65	1.5	283	40	86.7	24.0	23.3	25.9
16		93	1.8	283	40	121.9	23.6	25.8	28.5
17		92	1.7	303	40	26.0	5.0	4.7	8.0
18		145	1.8	303	40	73.4	9.0	8.3	12.4
19		195	1.9	303	40	110.5	10.1	11.4	15.5
20	*Ng et al.* [2006]	108	0.6	293	11	158	26.0	18.1	19.4
21	*Presto et al.* [2005a, 2005b]	10.8	0.54	295	300	0.96	1.6	0.2	0.8
22		11.8	0.28	295	300	0	0.	0.3	1.0
23		15	1.1	295	300	3.64	4.4	0.5	3.0
24		20.4	0.45	295	300	0	0.	0.8	5.6
25		20.6	1.9	295	300	5.63	4.9	1.0	7.1
26		152	17	295	300	143	16.9	14.8	26.5
27		156	26	295	300	164	18.9	14.8	26.8
28		205	32	295	300	260	22.8	11.8	25.9

[a]The columns provide the reacted α-pinene, the ratio of reacted α-pinene to initial NOx, temperature (T), the photolysis rate of NO_2, the measured aerosol mass (Mo), the observed mass yields of SOA (Y_{exp}), and the modeled mass yields using the original mechanism (Y_A), and the mechanism modified with additional acids (Y_B). See text for details.

section for the description of the initial conditions in these experiments). In all cases, the model captures very well the ozone buildup seen in the experiments. A slight underestimation can be noted for the simulated D(O_3 - NO) in one experiment (ETC420) after 2–3 hours, which might be related to the treatment of generic compounds in BOREAM. The time-dependent decay of α-pinene is very well reproduced by the model for both the *Kamens and Jaoui* [2001] experiments (see Figure 9 in the next section) and the SAPRC experiments (not shown).

3.2. Description of the Experiments Used to Validate SOA Formation

[31] Table 3 summarizes the photo-oxidation experiments simulated in this work. High NO_x conditions prevailed in these experiments, with the exception of a couple of experiments conducted by Presto et al.. No acidic seed particles were used in these experiments. When reported, relative humidity was generally low (<40%), except in the series of *Takekawa et al.* [2003] (60%) and *Ng et al.* [2006] (43%). Relative humidity was not reported for the *Hoffmann et al.* [1997] experiments. The UV/visible lamps used in these studies radiate primarily in the range 300–400 nm, to the exception of the lamps used by *Nozière et al.* [1999]. Their emission spectrum (or the solar spectrum in the case of outdoor chambers experiments) has been used to derive the wavelength-dependent radiative fluxes. For the experiments of *Nozière et al.* [1999], *Takekawa et al.* [2003] and *Ng et al.* [2006], the measured photolysis rate of NO_2 is used to calibrate the radiative fluxes. Time-dependent photorates are calculated in the experiments by *Kamens and Jaoui* [2001], and adjusted to match the observed degradation rate of α-pinene.

[32] The actinic fluxes in the experiments by *Presto et al.* [2005a, 2005b] are adjusted in order to maintain a relatively high NO/NO_2 ratio, as reported by these authors, and implying unusually high photorates ($J(NO_2)$ on the order of 0.03 s^{-1}). When information regarding the photorates is lacking, a standard atmospheric surface-level flux is adopted in the model. The SOA yields derived from the experiments are given in Table 3. Here an aerosol density ρ of 1 g cm^{-3} is assumed. The average molar weight MW_{om} is calculated online in the model, on the basis of the simulated aerosol composition. It ranges generally between 200 and 245 g mol^{-1}. Since SOA measurements are usually volume measurements, we correct the experimental SOA yields and mass concentrations reported in the literature with our values of ρ and MW_{om}. These data are also corrected for the losses on the walls. These are of the order of 0.2 h^{-1} in these series of experiments and are quite significant since the SOA reported in Table 3 is formed after a couple of hours.

3.3. Discussion of the Results

[33] The experimental and modeled SOA yields are compared on Figure 8, for 3 different versions of the chemical mechanism. The modeled yields indicated on Figure 8 represent the maximum value of the yield during the course of the experiment, corrected for wall losses, except in the case of the *Nozière et al.* [1999] experiments where the yields are estimated at the last experimental sampling time, and the cases of the *Ng et al.* [2006] and

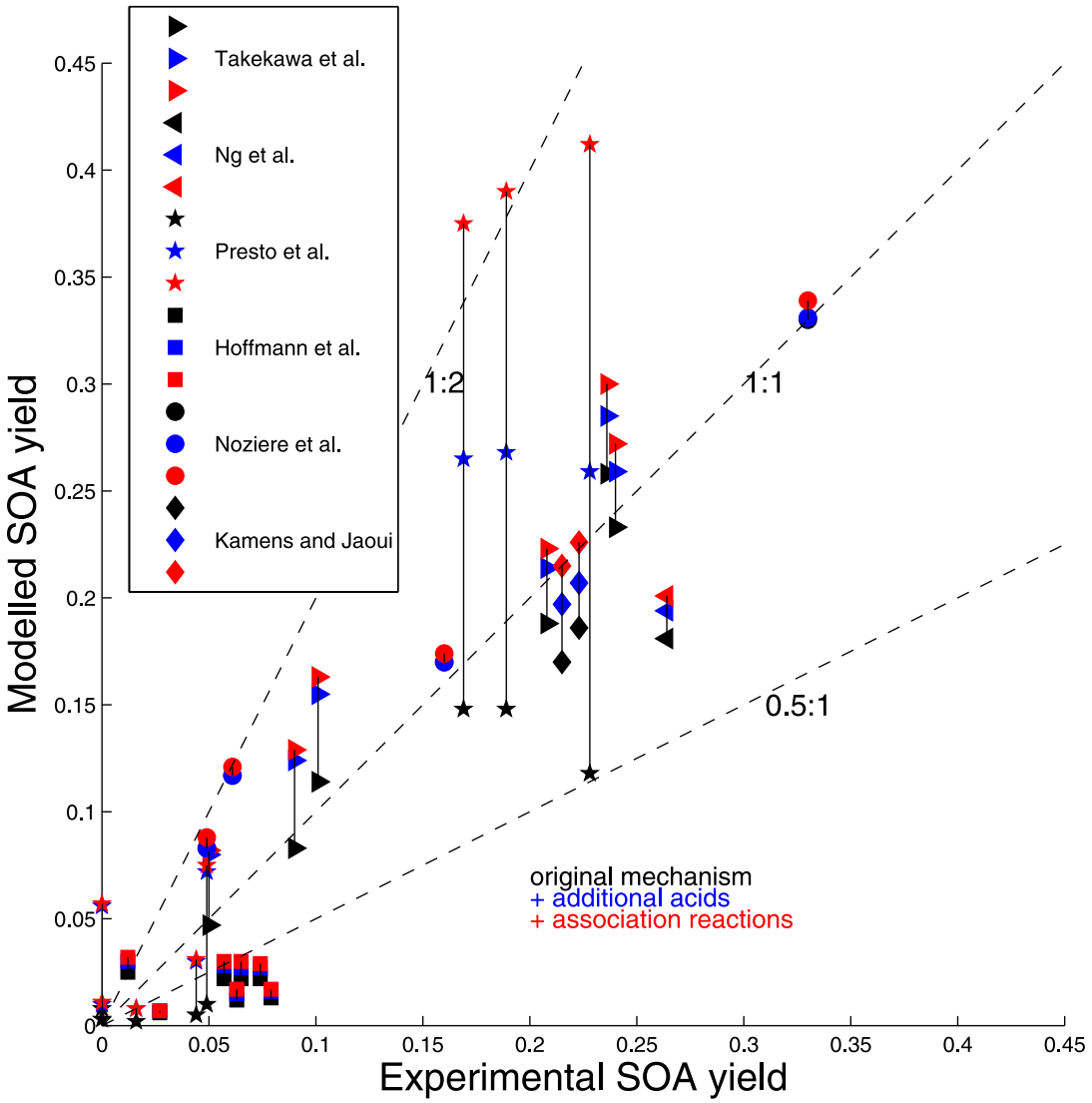

Figure 8. Measured versus modeled aerosol mass yields in the experiments reported in Table 3. Model results with the standard mechanism are indicated in black, results with the additional acids are indicated in blue, and results with additional acids and with association reactions of aldehydes and hydroperoxides are indicated in red (see text for details).

Kamens and Jaoui [2001] experiments, for which no wall loss correction is applied. Ozone is calculated to be the dominant oxidant (>85%) in the *Presto et al.* [2005a, 2005b] series, because of the use of the OH-scavenger 2-butanol (10 ppm). In the other experiments, OH, O_3 and NO_3 contribute typically to 50%, 40% and 10% of the total α-pinene sink, respectively, except in the work by *Hoffmann et al.* [1997], where NO_3 contributes to 20%, and in the work by *Nozière et al.* [1999], where OH is the only significant oxidant. With all 3 model versions, BOREAM reproduces fairly well the observations, with deviations of typically a factor of 2 or less. When the original mechanism is used (black symbols in Figure 8), the model performs best for the experiments with the highest initial VOC concentration, with deviations almost always lower than 50%, but it significantly underestimates the yields in most low-VOC experiments of *Presto et al.* [2005a] and *Hoffmann et al.* [1997], by factors of 2 or more. This implies that the current mechanism would most probably underestimate the SOA yields in atmospheric conditions.

[34] Including additional acids in the ozonolysis mechanism leads to a significant increase of the yields, except for the *Nozière et al.* [1999] series. The increase is largest (factor of 3 to 8) for the low-VOC *Presto et al.* [2005a, 2005b] experiments, where ozonolysis is the main α-pinene sink. For most of these experiments, the modified mechanism brings the model much closer to the observations. For the two *Presto et al.* [2005a, 2005b] experiments with the lowest initial VOC/NOx ratio (0.28 and 0.45), however, the model overestimates the yields (to about 1% and 7%), which were below the detection limit in the experiments. This is probably a consequence of using an acid production pathway adjusted to reproduce yields observed in low-NOx dark experiments [*Yu et al.*, 1999]. It has been previously observed that extrapolating yields from low-NOx dark

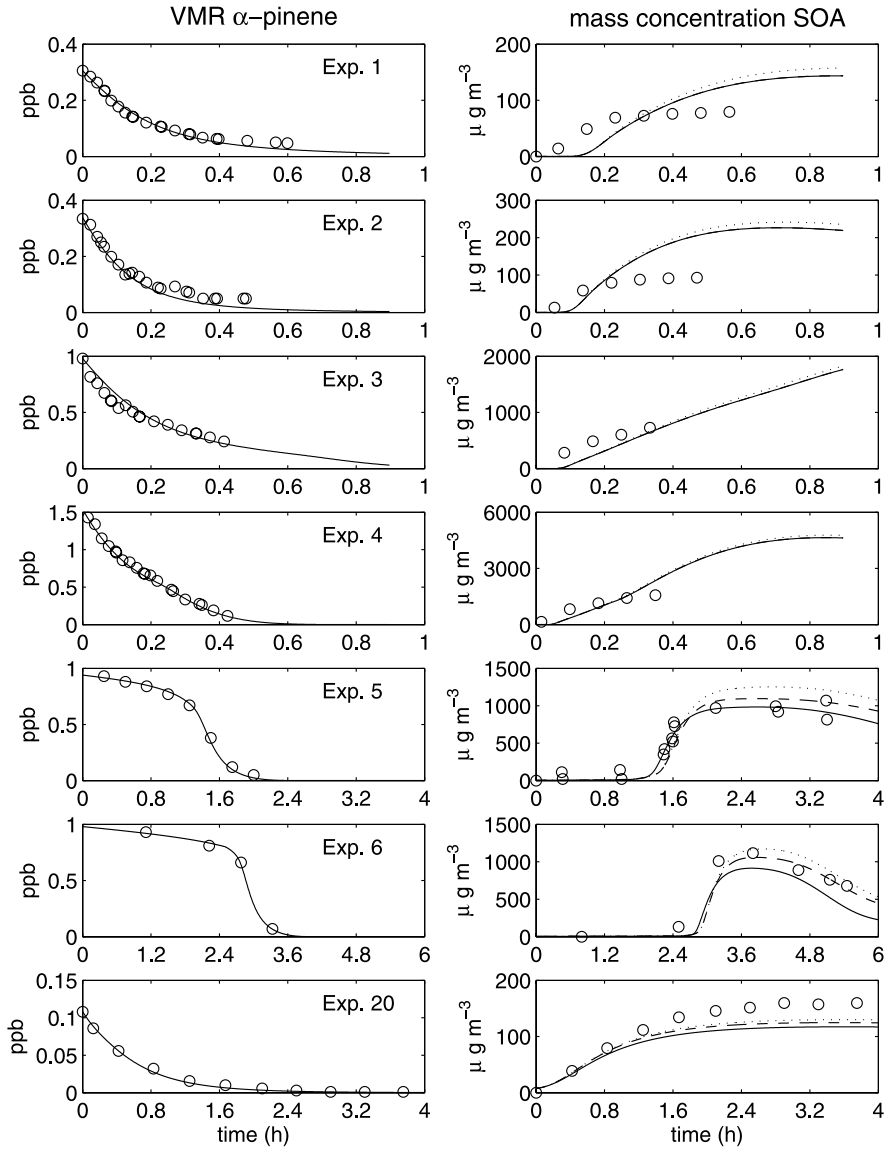

Figure 9. Time-dependent measured (circles) versus simulated (curves) concentrations of (left) α-pinene and (right) SOA in experiments 1–4 [*Nozière et al.*, 1999], 5–6 [*Kamens and Jaoui*, 2001] and 20 [*Ng et al.*, 2006] (see Table 3). The model results are obtained with the standard mechanism (solid lines), with the additional acids (dashed), and with additional acids and association reactions in the aerosol (dotted). See text for details.

experiments to photo-oxidation conditions in presence of NOx might lead to SOA overestimation [*Presto and Donahue*, 2006], probably because the production of hydroxypinonic acid and possibly other compounds is suppressed in the presence of NOx [*Presto et al.*, 2005b]. The inclusion of additional acids also leads to some overestimation of the yields in several *Takekawa et al.* [2003] and (high-VOC) *Presto et al.* [2005a, 2005b] experiments. The inclusion of association reactions has a minor impact on the yields in most cases, except for the high-VOC *Presto et al.* [2005a, 2005b] experiments, where SOA yields are increased by about one third, because of the large VOC/NOx ratios (up to about 20) used in these experiments, which led to large hydroperoxide yields favoring peroxyhemiacetal formation.

[35] Comparison of the simulations with the few available temporal profiles of observed concentrations (Figure 9) shows that the model can reproduce the SOA formation rates in diverse conditions, although the aerosol formation starts later in the model than in the observations in the *Nozière et al.* [1999] experiments.

[36] The temporal evolution of the molar ratios of the top species contributing to the modeled SOA is displayed on Figure 10 for experiment 3, from the *Nozière et al.* [1999] series, and experiment 28, from *Presto et al.* [2005a, 2005b] (see Table 3). The species structures are displayed in Figure 11. In experiment 3, where α-pinene is almost exclusively oxidized by OH, the compounds which appear first in the aerosol are hydroperoxide compounds generated from the H-shift of a peroxy radical in the OH-initiated oxidation mechanism, as discussed in section 2.2 (see Figure 2). A triol compound is also seen to contribute significantly (about 10%) in the first stage of the experi-

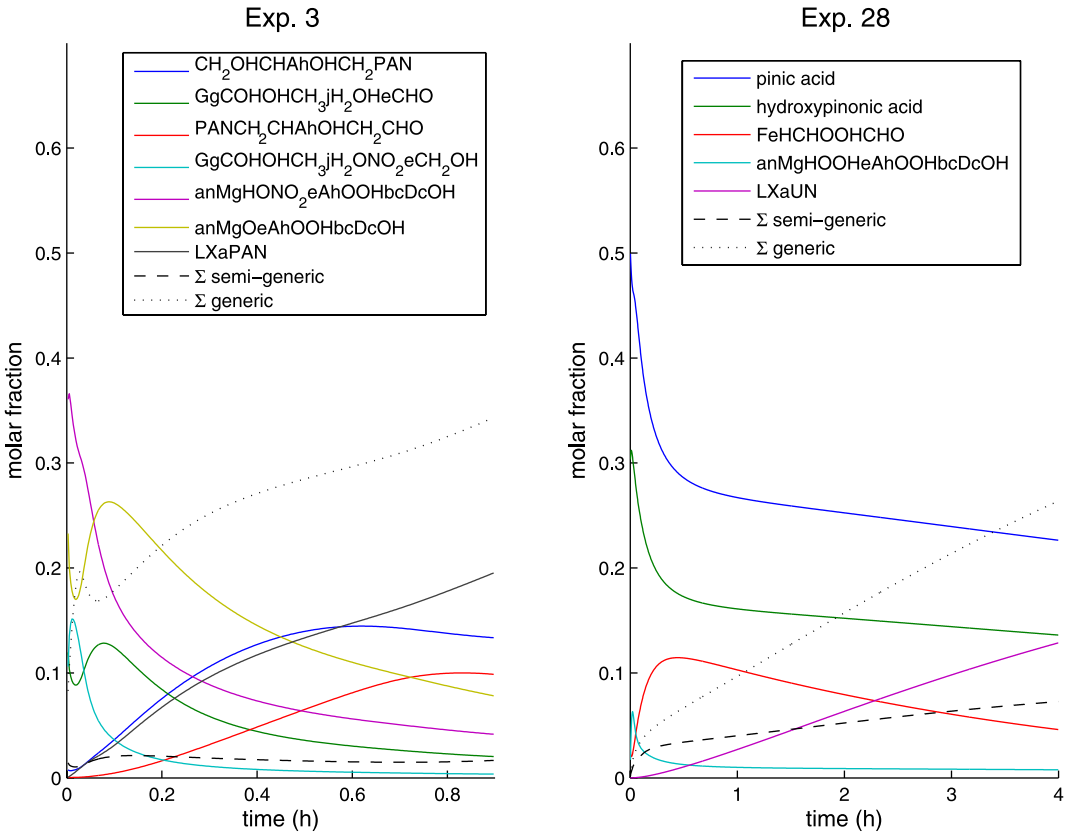

Figure 10. Time-dependent molar ratios of the main contributors to the simulated SOA in the experiments 3 [*Nozière et al.*, 1999] and 28 [*Presto et al.*, 2005a]. The structures of the compounds are given in Figure 11. The dotted and dashed lines represent the total molar ratio of generic and semigeneric species, respectively.

ment. Later in the experiment, other compounds contribute significantly, mostly made of nitrates and PAN-like compounds. Generic compounds (mostly PANs) contribute to about 30% of the total SOA at the end of the experiment.

[37] In experiment 28, pinic acid and hydroxy pinonic acid (which were included as an additional pathway of a Criegee Intermediate in the ozonolysis mechanism) are by far the main contributors, accounting to more than 40% of the total throughout the experiment. In both experiments 3 and 28, the contribution of generic compounds increases with time in the course of the experiment, to about 30% after 4 hours.

[38] As explained in section 2.3, mass is not conserved in the mechanism. For most experiments, this loss amounts to about 2–5%/h on a carbon basis. Important exceptions are the cases of *Hoffmann et al.* [1997] (~9%/h) and especially the experiments of *Nozière et al.* [1999] with a mean carbon loss rate of about 40%/h. The large carbon loss in this last case is caused by the very high H_2O_2 levels and the subsequent large oxidation rate. The loss of mass implies an underestimation of the modeled SOA yields, which might partly explain the SOA underestimation in the case of the *Hoffmann et al.* [1997] experiments, which lasted for several hours, although another possible cause for underestimation in these experiments might be heterogeneous and/or particle phase chemistry. In the case of the *Nozière et al.* [1999] experiments, however, the significant mass loss (on the order of 20% at the latest sampling time used here for calculating the SOA yields) implies that the apparent SOA overestimation by the model might be worse than is actually seen in Figure 8.

[39] The composition of the modeled SOA for different laboratory conditions is presented in Figure 12. The version of the mechanism modified to include additional acids has been used for these results. The aerosol is seen to be primarily made of multifunctional compounds: the sum of the molar ratios of the chemical functionalities in the particulate phase is equal to about 2 in most conditions. The fraction represented by generic (LX) compounds is found to be significant, but not dominant in any case. This would not be true at later times, e.g., after one or several days, when most gas phase as well as particulate primary products would have had enough time to be oxidized. Mass balance would also be very poor at such large timescales.

[40] PAN-like compounds are found to be a significant contribution to SOA in many experiments. Note that their formation in the oxidation of α-pinene by OH in presence of NO_x has been validated by comparisons with observations in the *Nozière et al.* [1999] experiments [*Capouet et al.*, 2004]. The large molar ratio of hydroperoxides (almost 0.3) calculated in the aerosol formed in the *Nozière et al.* [1999] experiments result almost exclusively from the newly proposed reaction sequence displayed in Figure 2, and discussed in section 2.2. In the other experiments,

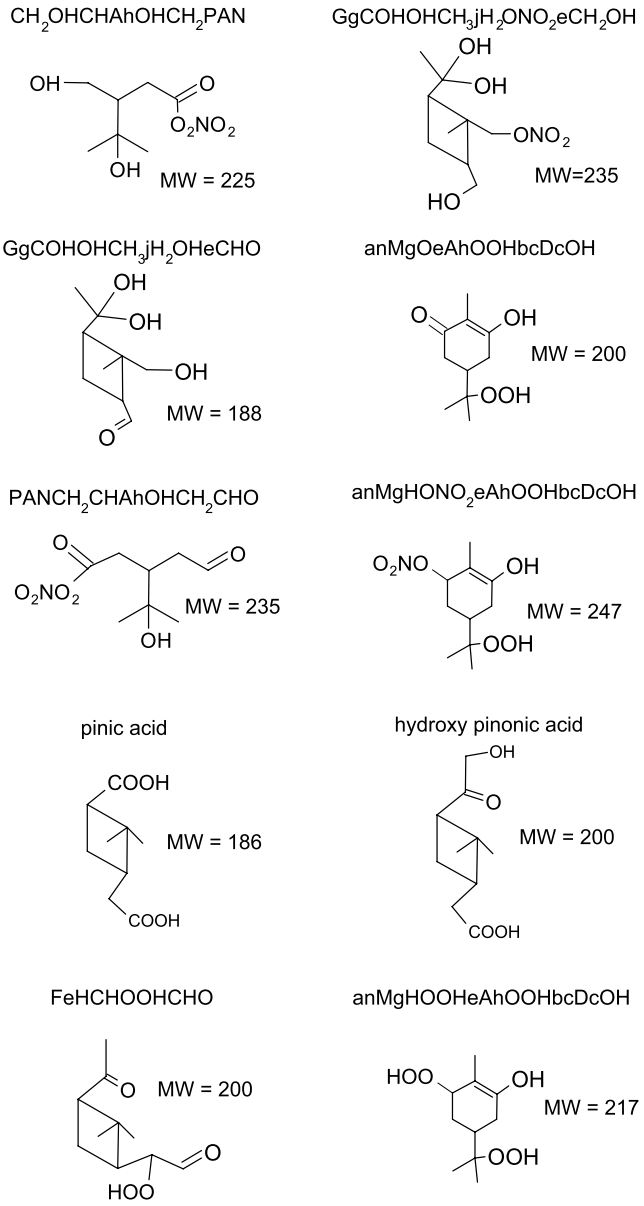

Figure 11. Explicit compounds contributing most to the modeled SOA in several experiments (see Figure 10). Their molecular masses are also indicated.

which were conducted with higher VOC/NO_x ratios, hydroperoxides are mostly formed from RO_2 + HO_2 reactions. Although the relative importance of this channel among the reactions involving RO_2 is generally small, it represent an important contribution to the production of condensable compounds in our model calculations. It contributes even more to the aerosol growth in the high-VOC *Presto et al.* [2005a, 2005b] experiments. The contribution of hydroperoxides to the modeled SOA would be even higher if the exceptionally low vapor pressure of a hydroxy hydroperoxide measured by *Tobias et al.* [2000] had been taken into account in the vapor pressure prediction method [*Capouet and Müller*, 2006], resulting in hydroperoxide vapor pressures about 3 times lower, similar to the estimation used by the modeling study of *Bonn et al.* [2004]. Organic acids are dominant in the aerosol formed in the *Presto et al.* [2005a, 2005b] experiment, where they represent between 50% and 70% of the SOA mass. Note that their contribution would be much lower (<10%) with the original version of the mechanism.

[41] The SOA yields are influenced by many factors, including the relative contributions of each oxidant to the sink of α-pinene, the VOC and NO_x abundances, the photorates, the oxidant abundance, and temperature. The ozonolysis of α-pinene produces more carboxylic acids and PAN-like compounds (when NO_x is available) than the OH- and the NO_3- initiated oxidations. Because of the low volatility of such compounds, and to the high volatility of the main primary product in the oxidation by OH as well as by NO_3, ozonolysis is expected to contribute more to SOA formation than the other oxidation pathways. This is confirmed by numerical experiments in which the same amount of α-pinene (30 ppbv) is allowed to react with only one oxidant. In agreement with *Griffin et al.* [1999a], ozonolysis is found to contribute about twice more to aerosol formation than OH oxidation, and the NO_3 channel is found to be negligible.

[42] In accordance with the absorptive partitioning theory (equation (15)), the SOA yield increases with the organic aerosol concentration ([M_o]) and therefore with the amount of precursor hydrocarbon which has reacted. This is illustrated in Figure 13 which summarizes the dependence of the yield on both the reacted VOC amount and the VOC/NO_x ratio. Figure 13 displays the calculated aerosol yield in a series of simulations with different VOC and NOx initial conditions, at 295 K, and with photodissociation rates calculated for surface-level atmospheric conditions (solar zenith angle of 45). The mechanism modified for the yield of low-volatility acids is used in these calculations. The yield of SOA is seen to increase when the VOC/NO_x ratio is increased, in agreement with laboratory studies [e.g., *Odum et al.*, 1996; *Presto et al.*, 2005b]. For large initial VOC concentrations (>60 ppbv), and VOC/NO_x ratios larger than 1, the calculated yield decreases with increasing VOC/NO_x, because of the incomplete α-pinene consumption in these conditions, since ozone cannot be efficiently produced from the oxidation of α-pinene at such low NO_x conditions. The dependence of the SOA yield on NO_x is especially pronounced for VOC/NO_x ratios lower than one. For example, for [VOC] = 20 or 100 ppbv, the yield increases by a factor of 2, from 1.5% and 10% for a ratio of 0.1 to 3% and more than 20% for a ratio of 1. This is a consequence of the lower volatilities of the hydroperoxides formed at lower NO_x levels. The yield of the main carboxylic acids (pinic and hydroxy pinonic acid) are NO_x-independent in these calculations, whereas there is evidence that at least hydroxy pinonic acid formation is decreased by the presence of NO_x [*Presto et al.*, 2005a]. Therefore the SOA yields shown on Figure 13 are probably overestimated at the lowest values of the VOC/NO_x ratio.

[43] The aerosol yields measured in the experiments by *Nozière et al.* [1999] are relatively large in spite of the high NO_x levels and the dominance of OH as α-pinene oxidant. The main reason for this is the large initial VOC concentrations used (Table 3). However, the comparison between SOA yields from different experiments is complicated

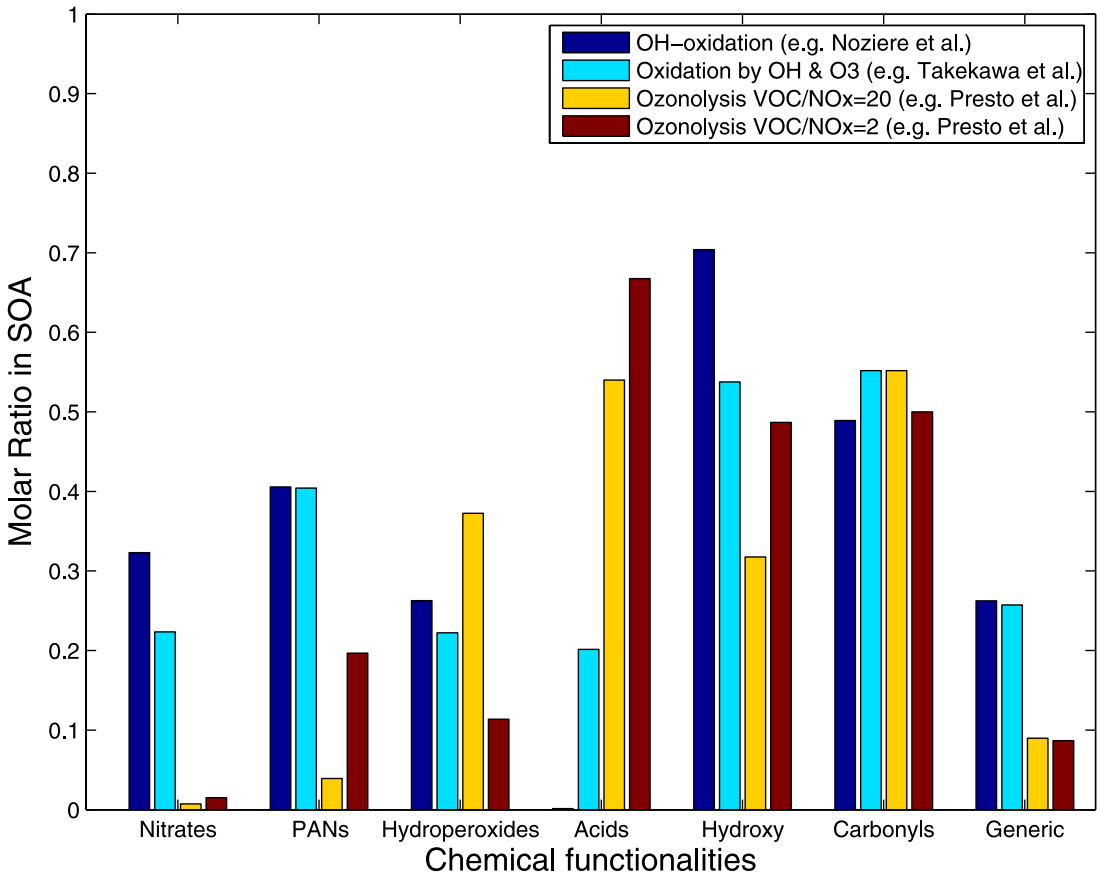

Figure 12. Composition of the modeled SOA, when using the mechanism modified to include low-volatility organic acids.

because of the great influence of the photolysis rates and the oxidant levels, as discussed below.

[44] Sensitivity tests with the model (Figure 14) show that, whereas a reduction of the light intensity has little effect on the SOA yield upon complete oxidation of α-pinene, a strong enhancement of the photolysis rates ($J(NO_2) = 300 \times 10^{-4}$ s^{-1}) increases the sink of the gaseous products, generating more volatile compounds and causing a rapid decline of the SOA mass. The reduction reaches a factor of 2 after 8 hours of simulations, compared to the

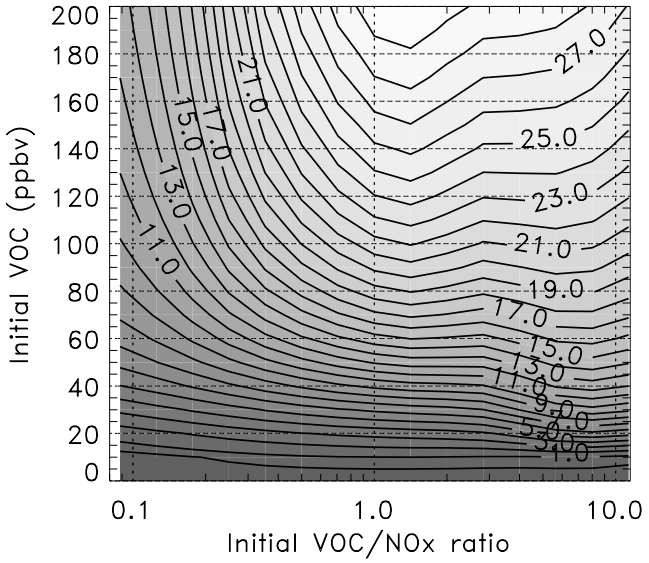

Figure 13. SOA mass yield as function of the initial VOC concentration (in ppbv) and the VOC/NOx ratio at 295 K. The photorates are estimated for typical atmospheric conditions (solar zenith angle of 45°).

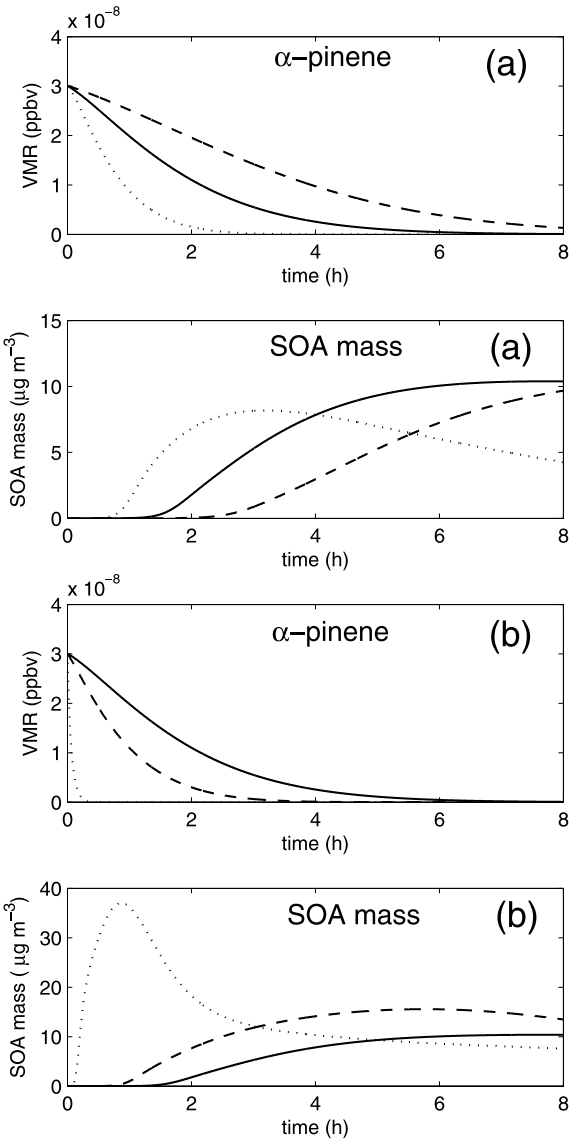

Figure 14. Model simulations of the oxidation of 30 ppb α-pinene in presence of 60 ppb NOx in different oxidative conditions. Temperature is 295 K, and the standard simulation uses photorates calculated for atmospheric conditions (solar zenith angle of 45°). (a) Varied photorates, with $J(NO_2) = 80 \times 10^{-4}$ s^{-1} (standard, solid lines), 300×10^{-4} s^{-1} (dotted lines) and 30×10^{-4} s^{-1} (dashed lines). (b) Standard photorates (solid lines), same with 200 ppb H_2O_2 added (dashed lines), and $J_{NO2} = 300 \times 10^{-4}$ s^{-1} and 800 ppb O_3 added (dotted lines).

standard case ($J(NO_2) = 80 \times 10^{-4}$ s^{-1}). The maximum SOA concentration is slightly reduced in these conditions.

[45] In the work by *Nozière et al.* [1999], the use of the OH precursor H_2O_2 with lamps emitting primarily around 253.7 nm leads to very high OH levels, and therefore to a rapid oxidation of the relatively volatile primary products. These reactions generate a large diversity of secondary products, from simple structures resulting from decomposition processes to complex multifunctional species having low vapor pressures and contributing to the aerosol growth. The model results shown in Figure 14b illustrate this effect. The OH-level enhancement by addition of H_2O_2 (dashed lines) is found to increase the production of SOA. This explains in part the high yields found by *Nozière et al.* [1999]. In one case (experiment 4), the calculated NO concentration drops rapidly to levels favoring the production of hydroperoxides, which leads to a further increase in the SOA yield. In the experiments by the other groups, the larger photolysis rate for NO_2 prevents such a rapid decline of the NO levels, except in *Presto et al.* [2005a, 2005b], where the fast α-pinene oxidation due to the large initial ozone concentrations used induce a fast conversion of NO to NO_2 not compensated by the large NO_2 photolysis rate, according to the model calculations.

[46] *Jenkin* [2004] and *Chen and Griffin* [2005] have simulated the formation of SOA in laboratory experiments of α-pinene degradation using the MCM and the CACM mechanisms, respectively. These studies found it necessary to increase the partitioning coefficients of the products by factors ranging between 120 and 1000 in order to match the observed SOA formation. Differences in the vapor pressure estimations of the products might partly explain the higher SOA yields and the better agreement with the observations in our model results. For example, the vapor pressures estimated by *Jenkin* [2004] for pinonic and pinic acid at 298 K are about 1 and 2 orders of magnitude higher than in our work, respectively, as discussed by *Capouet and Müller* [2006]. Another important reason for our higher SOA yields is the more explicit treatment adopted in our mechanism for the chemistry of primary products. The explicit description of a larger number of oxidation channels for the products generates a large variety of products with different volatilities. For example, the reaction of OH with $CH(O)CH_2C(O)CH_2OOH$ (Table 2) proceeds by 3 possible channels producing among others L10KPC(O)O2, precursor of low-volatility products, as well as much more volatile carbonyls. In contrast, the MCM mechanism considers only 1 channel (corresponding to our reaction (R2) in Table 2), which generates a relatively volatile carbonyl compound.

[47] The calculated temperature dependence of the SOA yield is illustrated in Figure 15. SOA formation is calculated to be favored by low temperatures. The primary reason for

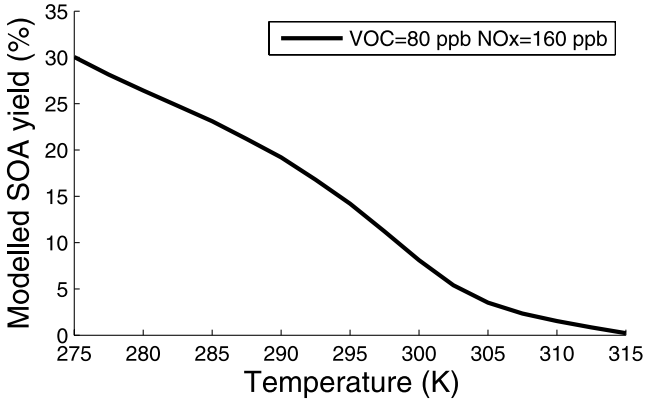

Figure 15. Temperature dependence of the modeled SOA yield (in %) for 80 ppbv α-pinene and 160 ppbv NOx, with photorates calculated for atmospheric conditions (solar zenith angle of 45°).

this behavior is the temperature dependence of the vapor pressures of the condensable products. A second reason is the influence of temperature on gas phase chemistry, e.g., the increased stability of PAN-like compounds at low temperatures. These results are in qualitative, if not quantitative agreement with laboratory investigations of the α-pinene/O_3 system [e.g., *Pathak et al.*, 2007] and references therein) which suggests a weaker temperature dependence of the yields, in particular above 15°C.

4. Conclusions

[48] A detailed α-pinene oxidation mechanism coupled to a gas/particle partitioning module has been tested against a large number of photo-oxidation experiments, and used to explore the dependence of SOA yields to several parameters. The average bias between the calculated and observed mass yields of SOA is small, in contrast with previous modeling studies which found it necessary to increase the partitioning coefficients by several orders of magnitude in order to match the observed SOA yields. The higher yields calculated by BOREAM are partly due to the more detailed treatment adopted for the gas phase degradation of the primary products. Given the importance of this chemistry for SOA production, more efforts should be devoted in the future to further improve its representation in models. A large underestimation of SOA formation rates is found at low initial VOC concentration when using the standard version of the mechanism. It is very probably due to still unknown pathways for the formation of very condensable acids, like pinic acid and hydroxy pinonic acid, as shown by sensitivity calculations using a modified version of the mechanism. The model calculates that the particle phase, reversible association reactions of aldehydes and hydroperoxides have only a minor impact on the SOA yields in most cases, when using association rates derived from laboratory experiments. Other particle phase and/or heterogeneous chemical processes might possibly also play an important role in some experiments [e.g., from *Hoffmann et al.*, 1997], although it is not clear how this could be elucidated, given the speculative nature of these processes and the generally incomplete description of the laboratory experiments, e.g., regarding water content and the aerosol sampling times.

[49] In agreement with laboratory data [*Presto et al.*, 2005b], the model indicates that elevated NO_x levels decrease the SOA yields. In the real atmosphere, high NOx conditions are frequently associated with anthropogenic emissions. As illustrated by the global model calculations presented in section 2.1, an additional effect of NO_x emissions in the atmosphere is to enhance the levels of OH (due to the $NO+HO_2$ reaction) and NO_3 (due to NO_2+O_3) much more than the levels of O_3, resulting in lower ozonolysis contributions, and therefore lower SOA yields, since ozonolysis is confirmed in our calculations as the most favorable route to aerosol formation [*Griffin et al.*, 1999a]. Since hydroperoxides could be more condensable than assumed in our study, and since the yield of low-volatility acids might be overestimated in high NOx conditions when using reaction channels adjusted using low-NOx, dark chamber results, we conclude that anthropogenic NO_x emissions tend to decrease the biogenic SOA burden in the atmosphere, whereas anthropogenic emissions of other pollutants (e.g., particulate matter) might have the opposite effect [*Kanakidou et al.*, 2000; *Tsigaridis and Kanakidou*, 2007].

[50] **Acknowledgments.** This work has been made possible by grants of the Belgian Science Policy Office in the framework of the SPSD II programme (2001–2004) and the SSD programme (2006–2007).

References

Alvarado, A., J. Arey, and R. Atkinson (1998), Kinetics of the gas-phase reactions of OH and NO_3 radicals and O_3 with the monoterpene reaction products pinonaldehyde, caronaldehyde, and sabinaketone, *J. Atmos. Chem.*, *31*, 281–297.

Anderson-Sköld, Y., and D. Simpson (2001), Secondary organic aerosol formation in northern Europe, *J. Geophys. Res.*, *106*, 7257–7374.

Antonovskii, V. L., and V. A. Terent'ev (1967), Effect of the structure of hydroperoxides and some aldehydes on the kinetics of the noncatalytic formation of α-hydroxy peroxides, *Zh. Org. Khim.*, *3*, 1011–1013.

Aschmann, S. M., A. Reissel, R. Atkinson, and J. Arey (1998), Products of the gas phase reactions of the OH radical with α- and β-pinene in the presence of NO, *J. Geophys. Res.*, *103*, 25,553–25,561.

Atkinson, R., D. L. Baulch, R. A. Cox, J. N. Crowley, R. F. Hampson, R. G. Hynes, M. E. Jenkin, M. J. Rossi, and J. Troe (2005), Evaluated kinetic and photochemical data for atmospheric chemistry: Volume II—Reactions of organic species, *Atmos. Chem. Phys. Disc.*, *5*, 6295–7168.

Aumont, B., S. Szopa, and S. Madronich (2005), Modelling the evolution of organic carbon during its gas-phase tropospheric oxidation: Development of an explicit model based on a self generating approach, *Atmos. Chem. Phys.*, *5*, 2497–2517.

Baker, J., S. M. Aschmann, J. Arey, and R. Atkinson (2002), Reaction of stabilized criegee intermediates from gas-phase reactions with O_3 with selected alkenes, *Int. J. Chem. Kinet.*, *34*, 73–85.

Barnes, I., K. H. Becker, and T. Zhu (1993), Near UV absorption spectra and photolysis products of difunctional organic nitrates, possible importance as NO_x reservoirs, *J. Atmos. Chem.*, *17*, 353–373.

Berndt, T., O. Böge, and F. Stratmann (2003), Gas-phase ozonolysis of α-pinene: Gaseous products and particle formation, *Atmos. Environ.*, *37*, 3933–3945.

Bilde, M., and S. N. Pandis (2001), Evaporation rates and vapor pressures of individual aerosol species formed in the atmospheric oxidation of α- and β-pinene, *Environ. Sci. Technol.*, *35*, 3344–3349.

Bonn, B., and G. K. Moortgat (2002), New particle formation during α- and β-pinene oxidation by O_3, OH and NO_3, and the influence of water vapour: Particle size distribution studies, *Atmos. Chem. Phys.*, *2*, 183–196.

Bonn, B., R. von Kuhlmann, and M. Lawrence (2004), High contribution of biogenic hydroperoxides to secondary organic aerosol formation, *Geophys. Res. Lett.*, *31*, L10108, doi:10.1029/2003GL019172.

Bowman, F. M., J. R. Odum, J. H. Seinfeld, and S. N. Pandis (1997), Mathematical model for gas-particle partitioning of secondary organic aerosols, *Atmos. Environ.*, *31*, 3921–3931.

Capouet, M., and J.-F. Müller (2006), A group contribution method for estimating the vapour pressures of α-pinene oxidation products, *Atmos. Chem. Phys.*, *6*, 1455–1467.

Capouet, M., J. Peeters, B. Nozière, and J.-F. Müller (2004), Alpha-pinene oxidation by OH: Simulations of laboratory experiments, *Atmos. Chem. Phys.*, *4*, 2285–2311.

Carter, W. P. L. (2000), Documentation of the SAPRC-99 chemical mechanism for VOC reactivity assessment, final report to California Resources Board, contracts 92-329 and 95-308, Air Pollut. Res. Cent. and Coll. of Eng., Cent. for Environ. Res. and Technol., Univ. of Calif., Riverside, Calif. (Available at http://www.cert.ucr.edu/~carter/absts.htm#saprc99 and http://www.cert.ucr.edu/~carter/reactdat.htm)

Carter, W. P. L., and F. W. Lurmann (1991), Evaluation of a detailed gas-phase atmospheric reaction mechanism using environmental chamber data, *Atmos. Environ.*, *25*, 2771–2806.

Chen, J., and R. J. Griffin (2005), Modeling secondary organic aerosol formation from oxidation of α-pinene, β-pinene, and d-limonene, *Atmos. Environ.*, *39*, 7731–7744.

Chew, A. A., and R. Atkinson (1998), Measurement of OH radical formation from the reaction of ozone with several biogenic alkenes, *J. Geophys. Res.*, *103*, 25,533–25,539.

Christoffersen, T. S., et al. (1998), Cis-pinic acid, a possible precursor for organic aerosol formation from ozonolysis of α-pinene, *Atmos. Environ.*, *32*, 1657–1661.

Chung, S. H., and J. H. Seinfeld (2002), Global distribution and climate forcing of carbonaceous aerosols, *J. Geophys. Res.*, *107*(D19), 4407, doi:10.1029/2001JD001397.

Damian-Iordache, V., A. Sandu, F. A. Potra, G. R. Carmichael, and M. Damian-Iordache (1995), KPP—A symbolic preprocessor for chemical kinetics, user's guide, technical report, Cent. for Global and Reg. Environ. Res., Univ. of Iowa, Iowa City.

Derwent, R. G., W. J. Collins, M. E. Jenkin, C. E. Johnson, and D. S. Stevenson (2003), The global distribution of Secondary Particulate Matter in a 3-D Lagrangian Chemistry Transport Model, *J. Atmos. Chem.*, *44*, 57–95.

Desai, J., J. Heicklen, A. Bahta, and R. Simonaitis (1986), The photooxidation of *i*-C_3H_7CHO vapour, *J. Photochem.*, *34*, 137–164.

Dindorf, T., U. Kuhn, L. Ganzeveld, G. Schebeske, P. Ciccioli, C. Holzke, R. Köble, G. Seufert, and J. Kesselmeier (2006), Significant light and temperature dependent monoterpene emissions from European beech (*Fagus sylvatica* L.) and their potential impact on the European volatile organic compound budget, *J. Geophys. Res.*, *111*, D16305, doi:10.1029/2005JD006751.

Fantechi, G., L. Vereecken, and J. Peeters (2002), The OH-initiated atmospheric oxidation of pinonaldehyde: Detailed theoretical study and mechanism construction, *Phys. Chem. Chem. Phys.*, *4*, 5795–5805.

Fick, J., L. Pommer, C. Nilsson, and B. Anderson (2003), Effect of OH radicals, relative humidity, and time on the composition of the products formed in the ozonolysis of alpha-pinene, *Atmos. Environ.*, *37*, 4087–4096.

Fuller, E. N., K. Ensley, and C. J. Giddings (1969), Diffusion of halogenated hydrocarbons in helium, *J. Phys. Chem.*, *73*, 3679–3685.

Gao, S., et al. (2004), Particle phase acidity and oligomer formation in Secondary Organic Aerosol, *Environ. Sci. Technol.*, *38*, 6582–6589.

Glasius, M., M. Lahaniati, A. Calogirou, D. Di Bella, N. R. Jensen, J. Hjorth, D. Kotzias, and B. R. Larsen (2000), Carboxylic acids in secondary aerosols from oxidation of cyclic monoterpenes by ozone, *Environ. Sci. Technol.*, *34*, 1001–1010.

Griffin, R. J., D. R. Cocker III, R. C. Flagan, and J. H. Seinfeld (1999a), Organic aerosol formation from the oxidation of biogenic hydrocarbons, *J. Geophys. Res.*, *104*, 3555–3567.

Griffin, R. J., D. R. Cocker III, and J. H. Seinfeld (1999b), Estimate of global atmospheric aerosol formation from the oxidation of biogenic hydrocarbons, *Geophys. Res. Lett.*, *26*, 2721–2724.

Griffin, R. J., D. Dabdub, M. J. Kleeman, M. P. Fraser, G. R. Cass, and J. H. Seinfeld (2002), Secondary organic aerosol 3. Urban/regional scale model of size- and composition-resolved aerosols, *J. Geophys. Res.*, *107*(D17), 4334, doi:10.1029/2001JD000544.

Guenther, A., et al. (1995), A global model of natural volatile organic compound emissions, *J. Geophys. Res.*, *100*, 8873–8892.

Guenther, A., T. Karl, P. Harley, C. Wiedinmyer, P. Palmer, and C. Geron (2006), Estimates of global terrestrial isoprene emissions using MEGAN (Model of Emissions of gases and Aerosols from Nature), *Atmos. Chem. Phys.*, *6*, 3181–3210.

Hakola, H., J. Arey, S. M. Aschmann, and R. Atkinson (1994), Product formation from the gas-phase reactions of OH radicals and O_3 with a series of monoterpenes, *J. Atmos. Chem.*, *18*, 75–102.

Hallquist, M., I. Wängberg, and E. Ljungström (1997), Atmospheric fate of carbonyl oxidation products originating from α-pinene and δ^3-carene: Determination of rate of reaction with OH and NO_3 radicals, UV absorption cross sections, and vapor pressure, *Environ. Sci. Technol.*, *31*, 3166–3172.

Hallquist, M., I. Wängberg, E. Ljungström, I. Barnes, and K.-H. Becker (1999), Aerosol and product yields from NO_3 radical-initiated oxidation of selected monoterpenes, *Environ. Sci. Technol.*, *33*, 553–559.

Hatakeyama, S., K. Izumi, T. Fukuyama, H. Akimoto, and N. Washida (1991), Reaction of OH with α-pinene and β-pinene in air: Estimate of global CO production from the atmospheric oxidation of terpenes, *J. Geophys. Res.*, *96*, 947–958.

Hermans, I., J.-F. Müller, T. L. Nguyen, P. A. Jacobs, and J. Peeters (2005), Kinetics of alfa-hydroxy-alkylperoxyl radicals in oxidation processes. HO_2-initiated oxidation of ketones/aldehydes near the tropopause, *J. Phys. Chem. A*, *109*, 4303–4311.

Hoffmann, T., J. R. Odum, F. Bowman, D. Collins, D. Klockow, R. C. Flagan, and J. Seinfeld (1997), Formation of organic aerosols from the oxidation of biogenic hydrocarbons, *J. Atmos. Chem.*, *26*, 189–222.

Jang, M., and R. M. Kamens (1998), A thermodynamic approach for modeling partitioning of semivolatile organic compounds on atmospheric particulate matter: Humidity effects, *Environ. Sci. Technol.*, *32*, 1237–1243.

Jang, M., and R. M. Kamens (1999), Newly characterized products and composition of secondary aerosols from the reaction of α-pinene with ozone, *Atmos. Environ.*, *33*, 459–474.

Jenkin, M. E. (2004), Modelling the formation and composition of secondary organic aerosol from α-pinene and β-pinene ozonolysis using MCM v3, *Atmos. Chem. Phys.*, *4*, 1741–1757.

Jenkin, M. E., D. E. Shallcross, and J. N. Harvey (2000), Development and application of a possible mechanism for the generation of cis-pinic acid from the ozonolysis of α- and β-pinene, *Atmos. Environ.*, *34*, 2837–2850.

Johnson, D., M. E. Jenkin, K. Wirtz, and M. Martin-Reviejo (2005), Simulating the formation of secondary organic aerosol from the photooxidation of aromatic hydrocarbons, *Atmos. Environ.*, *2*, 35–48.

Kalberer, M., et al. (2004), Identification of polymers as major components of atmospheric organic aerosols, *Science*, *303*, 1659–1662.

Kamens, R., and M. Jaoui (2001), Modeling aerosol formation from α-pinene + NO_x in the presence of natural sunlight using gas-phase kinetics and gas-particle partitioning theory, *Environ. Sci. Technol.*, *35*, 1394–1405.

Kamens, R., M. Jang, C.-J. Chien, and K. Leach (1999), Aerosol formation from the reaction of α-pinene and ozone using a gas-phase kinetics-aerosol partitioning model, *Environ. Sci. Technol.*, *33*, 1430–1438.

Kanakidou, M., K. Tsigaridis, F. J. Dentener, and P. J. Crutzen (2000), Human-activity enhanced formation of organic aerosols by biogenic hydrocarbon oxidation, *J. Geophys. Res.*, *105*, 9243–9254.

Kesselmeier, J. (2004), Interactive comment on "Seasonal cycles of isoprene concentrations in the Amazonian rainforest" by C. R. Trostdorf et al., *Atmos. Chem. Phys. Disc.*, *4*, 528–530.

Koch, S., R. Winterhalter, E. Uherek, A. Kolloff, P. Neeb, and G. K. Moortgat (2000), Formation of new particles in the gas-phase ozonolysis of monoterpenes, *Atmos. Environ.*, *34*, 4031–4042.

Kubistin, D., et al. (2007), Hydroxyl radicals in the tropical troposphere during GABRIEL: Comparison of measurements with the box model MECCA, *Geophys. Res. Abstr.*, *9*, 07065.

Lack, D. A., X. X. Tie, N. D. Bofinger, A. N. Wiegand, and S. Madronich (2004), Seasonal variability of secondary organic aerosol: A global modeling study, *J. Geophys. Res.*, *109*, D03203, doi:10.1029/2003JD003418.

Lelieveld, J., and P. J. Crutzen (1991), The role of clouds in tropospheric photochemistry, *J. Atmos. Chem.*, *12*, 229–267.

Ma, Y., T. Luciani, R. A. Porter, A. T. Russell, D. Johnson, and G. Martson (2007), Organic acid formation in the gas-phase ozonolysis of α-pinene, *Phys. Chem. Chem. Phys.*, *9*, 5084–5087, doi:10.1039/b709880d.

Madronich, S., and S. Flocke (1998), *Handbook of Environmental Chemistry*, edited by P. Boule, Springer, Heidelberg, Germany.

Müller, J.-F., T. Stavrakou, S. Wallens, A. B. Guenther, M. J. Potosnak, J. Rinne, B. Munger, and A. Goldstein (2007), Global isoprene emissions calculated based on MEGAN and a detailed canopy environment model, *Atmos. Chem. Phys. Disc.*, *7*, 15,373–15,407.

Neeb, P. (2000), Structure-reactivity based estimation of the rate constants for hydroxyl radical reactions with hydrocarbons, *J. Atmos. Chem.*, *35*, 295–315.

Ng, N. L., J. H. Kroll, M. D. Keywood, R. Bahreini, V. Varutbangkul, R. C. Flagan, and J. Seinfeld (2006), Contribution of first- versus second-generation products to secondary organic aerosols formed in the oxidation of biogenic hydrocarbons, *Environ. Sci. Technol.*, *40*, 2283–2297.

Nozière, B., I. Barnes, and K. H. Becker (1999), Product study and mechanisms of the reactions of α-pinene and of pinonaldehyde with OH radicals, *J. Geophys. Res.*, *104*, 23,645–23,656.

Odum, J. R., T. Hoffmann, F. Bowman, D. Collins, R. C. Flagan, and J. H. Seinfeld (1996), Gas/particle partitioning and secondary organic aerosol AMFs, *Environ. Sci. Technol.*, *30*, 2580–2585.

Pankow, J. F. (1994a), An absorption model of gas/particle partitioning of organic compounds in the atmosphere, *Atmos. Environ.*, *28*, 185–188.

Pankow, J. F. (1994b), An absorption model of gas/aerosol partitioning involved in the formation of secondary organic aerosol, *Atmos. Environ.*, *28*, 189–193.

Pathak, R. K., C. O. Stanier, N. M. Donahue, and S. N. Pandis (2007), Ozonolysis of α-pinene at atmospherically relevant concentrations: Temperature dependence of aerosol mass fractions (yields), *J. Geophys. Res.*, *112*, D03201, doi:10.1029/2006JD007436.

Paulson, S. E., M. Chung, A. D. Sen, and G. Orzechowska (1998), Measurement of OH radical formation from the reaction of ozone with several biogenic alkenes, *J. Geophys. Res.*, *103*, 25,533–25,539.

Peeters, J., L. Vereecken, and G. Fantechi (2001), The detailed mechanism of the OH-initiated atmospheric oxidation of α-pinene: A theoretical study, *Phys. Chem. Chem. Phys.*, *3*, 5489–5504.

Presto, A. A., and N. M. Donahue (2006), Investigation of α-pinene + ozone secondary organic aerosol formation at low total aerosol mass, *Environ. Sci. Technol.*, *40*, 3536–3543.

Presto, A. A., K. E. Huff Hartz, and N. M. Donahue (2005a), Secondary organic aerosol production from terpene ozonolysis: 1. Effect of UV radiation, *Environ. Sci. Technol.*, *39*, 7036–7045.

Presto, A. A., K. E. Huff Hartz, and N. M. Donahue (2005b), Secondary organic aerosol production from terpene ozonolysis: 2. Effect of NOx concentration, *Environ. Sci. Technol.*, *39*, 7046–7054.

Raber, W. H., and G. K. Moortgat (1995), *Progress and Problems in Atmospheric Chemistry*, edited by J. R. Barker, World Sci., Singapore.

Rickard, A. R., D. Johnson, C. D. McGill, and G. Marston (1999), OH yields in the gas-phase reactions of ozone with alkenes, *J. Phys. Chem. A*, *103*, 7656–7664.

Ruppert, L., K. H. Becker, B. Nozière, and M. Spittler (1999), *Transport and Chemical Transformation in the Troposphere*, edited by P. Borrell and P. M. Borrell, pp. 63–68, WIT Press, Southampton, U. K.

Sander, S. P., et al. (2006), Chemical kinetics and photochemical data for use in atmospheric studies, evaluation number 15, *JPL Publ. 06-2*, Jet Propul. Lab., Pasadena, Calif.

Saunders, S. M., M. E. Jenkin, R. G. Derwent, and M. J. Pilling (2003), Protocol for the development of the master chemical mechanism, MCM v3 (Part a): Tropospheric degradation of non-aromatic volatile organic compounds, *Atmos. Chem. Phys.*, *3*, 161–180.

Schurath, U., and K.-H. Naumann (2003), Chemical Mechanism Development (CMD), EUROTRAC-2 subproject, final report, 145 pp., Int. Sci. Secr.t, GSF-Natl. Res. Cent. for Environ. and Health, Munich, Germany.

Seinfeld, J., and S. N. Pandis (1998), *Atmospheric Chemistry and Physics*, John Wiley, New York.

Seinfeld, J., and J. F. Pankow (2003), Organic atmospheric particulate material, *Annu. Rev. Phys. Chem.*, *54*, 121–140.

Stavrakou, T., and J.-F. Müller (2006), Grid-based versus big region approach for inverting CO emissions using Measurement of Pollution in the Troposphere (MOPITT) data, *J. Geophys. Res.*, *111*, D15304, doi:10.1029/2005JD006896.

Tadic, J., I. Juranic, and G. K. Moortgat (2001a), Pressure dependence of the photooxidation of selected carbonyl compounds in air: n-butanal and n-pentanal, *J. Photochem. A*, *143*, 169–179.

Tadic, J., I. Juranic, and G. K. Moortgat (2001b), Photooxidation of *n*-hexanal, *Molecules*, *6*, 289–299.

Tadic, J., I. Juranic, and G. K. Moortgat (2002), Photooxidation of *n*-heptanal in air: Norrish type I and II processes and quantum yield total pressure dependency, *J. Chem. Soc. Perkin Trans.*, *2*, 135–140.

Takekawa, H., H. Minoura, and S. Yamazaki (2003), Temperature dependence of secondary organic aerosol formation by photo-oxidation of hydrocarbons, *Atmos. Environ.*, *37*, 3413–3424.

Tobias, H. J., and P. J. Ziemann (2000), Thermal desorption mass spectrometric analysis of organic aerosol formed from reactions of 1-tetradecene and O_3 in the presence of alcohols and carboxylic acids, *Environ. Sci. Technol.*, *34*, 2105–2115.

Tobias, H. J., K. S. Docherty, D. E. Beving, and P. J. Ziemann (2000), Effect of relative humidity on the chemical composition of Secondary Organic Aerosol formed from reactions of 1-tetradecene and O_3, *Environ. Sci. Technol.*, *34*, 2116–2125.

Tsigaridis, K., and M. Kanakidou (2007), Secondary organic aerosol importance in the future atmosphere, *Atmos. Environ.*, *41*, 4682–4692.

Tsigaridis, K., J. Lathière, M. Kanakidou, and D. H. Hauglustaine (2005), Naturally driven variability in the global secondary organic aerosol over a decade, *Atmos. Chem. Phys.*, *5*, 1891–1904.

Vereecken, L., and J. Peeters (2002), Enhanced H-atom abstraction from pinonaldehyde, pinonic acid, pinic acid, and related compounds: Theoretical study of C-H bond strengths, *Phys. Chem. Chem. Phys.*, *4*, 467–472.

Vereecken, L., T. L. Nguyen, I. Hermans, and J. Peeters (2004), Computational study of the stability of alpha-hydroperoxyl- or alpha-alkylperoxyl-substituted substituted alkyl radicals, *Chem. Phys. Lett.*, *393*, 432–436.

Vereecken, L., J.-F. Müller, and J. Peeters (2007), Low-volatility poly-oxygenates in the OH-initiated atmospheric degradation of *alpha*-pinene: Impact of non-traditional peroxy radical chemistry, *Phys. Chem. Chem. Phys.*, *9*, 5241–5248, doi:10.1039/b708023a.

Wängberg, I., I. Barnes, and K. H. Becker (1997), Product and mechanistic study of the reaction of NO_3 radicals with α-pinene, *Environ. Sci. Technol.*, *31*, 2130–2135.

Warscheid, B., and T. Hoffmann (2001), On-line measurements of α-pinene ozonolysis products using an atmospheric pressure chemical ionisation ion-trap mass spectrometer, *Atmos. Environ.*, *35*, 2927–2940.

Winterhalter, R., R. Van Dingenen, B. R. Larsen, N. R. Jensen, and R. Hjorth (2003), LC-MS analysis of aerosol particles from the oxidation of α-pinene by ozone and OH radicals, *Atmos. Chem. Phys. Disc.*, *3*, 1–39.

Yu, J., D. R. Cocker III, R. J. Griffin, R. C. Flagan, and J. H. Seinfeld (1999), Gas-phase ozone oxidation of monoterpenes: Gaseous and particulate products, *J. Atmos. Chem.*, *34*, 207–258.

M. Capouet, Belgian Agency for Radioactive Waste and Enriched Fissile Materials, B-1210 Brussels, Belgium.

K. Ceulemans, S. Compernolle, and J.-F. Müller, Belgian Institute for Space Aeronomy, Avenue Circulaire, 3, B-1180 Brussels, Belgium. (jean-francois.muller@aeronomie.be)

J. Peeters and L. Vereecken, Department of Chemistry, University of Leuven, Celestijnenlaan 200F, B-3000 Leuven, Belgium.